Bayesian age-depth modelling applied to varve and radiometric dating to optimize the transfer of an existing high-resolution chronology to a new composite sediment profile from Holzmaar (West-Eifel Volcanic Field, Germany)

Stella Birlo[1*], Wojciech Tylmann[2], Bernd Zolitschka[1]

1 - University of Bremen, Institute of Geography, GEOPOLAR, Bremen, Germany

2 - University of Gdańsk, Faculty of Oceanography and Geography, Gdańsk, Poland

*Corresponding author: sbirlo@uni-bremen.de

Abstract

This study gives an overview of different methods to integrate information from a varve chronology and radiometric measurements in the Bayesian tool Bacondifferent varve integration methods with Bacon. These techniques will become important for the future as technologies evolve with more sites being revisited for the application of new and high-resolution scanning methods. Thus, the transfer of existing chronologies will become necessary, because the recounting of varves will be too time consuming and expensive to be funded.

We introduce new sediment cores from Holzmaar (West-Eifel Volcanic Field, Germany), a volcanic maar lake with a well-studied varved record. Four different age-depth models (A-D) have been calculated for the new composite sediment profile (HZM19) using Bayesian statistics modelling with Bacon. All models incorporate new Pb-210 and Cs-137 dates for the top of the record, the latest calibration curve (IntCal20) for radiocarbon ages as well as the new age estimation for the Laacher See Tephra. Model A is based on previously published radiocarbon measurements only, while Models B-D integrate the previously published varve chronology (VT-99) with different approaches. Model B rests upon radiocarbon data, while parameter settings are obtained from sedimentation rates derived from VT-99. Model C is based on radiocarbon dates and on VT-99 as several normal-distributed tie-points, while Model D is segmented into four sections: Sections 1 and 3 are based on VT-99 only, whereas Sections 2 and 4 rely on Bacon age-depth models including additional information from VT-99. In terms of accuracy, the parameter-based integration Model B shows little improvement over the non-integrated approach, whereas the tie point-based integration Model C reflects the complex accumulation history of Holzmaar much better. Only the segmented and parameter-based age-integration approach of Model D adapts and improves VT-99 by replacing sections of higher counting errors with Bayesian modelling of radiocarbon ages and thus efficiently makes available the best possible and most precise age-depth model for HZM19. This approach will value all ongoing and high-resolution investigations for a better understanding of decadal-scale Holocene environmental and climatic variations.

Keywords: Lacustrine sediments, Varves, Bayesian age-depth modelling, Bacon, Radiometric dating

2

1. Introduction

Terrestrial archives from lakes have the potential to provide information about climate and the human history of its catchment area beyond instrumental and historical data (Berglund, 1986; Last and Smol, 2001a, b; Cohen, 2003). In the late 1980s, gravity coring (Kelts et al., 1986), piston coring (Nesje et al., 1987; Wright et al., 1984) and freeze coring techniques (Renberg and Hansson, 1993) for lacustrine sediment records have improved tremendously allowing a better quality of sediments to be recovered from modern lakes. Since then, the new fields of limnogeology and paleolimnology flourished with increasing demand of societies for documentation of natural background data related to questions around acid rain (e.g. Battarbee et al., 1990), environmental pollution (e.g. Renberg et al., 1994) and more and more with a focus on global climate change (e.g. Jenny et al., 2019).

To provide such information not only on local scales but also on larger regional to global scales, investigations from different sites need to be compared and linked. However, such correlations are only successful if the contributing archives are based on robust chronologies. Therefore, precise and reliable age-depth models are the basis for sedimentary investigations and reconstructions of environmental and climatic changes of the past, as only they ensure intra-site comparability and enable recognition of larger scale patterns. A reliable chronology ~~should~~ can be based on a combination of different dating techniques (multiple dating approach) such as radiometric dating, well-known events such as tephra layers (Turkey and Lowe, 2001; Davies, 2015), ~~layers (e.g., tephrochronology),~~ historic data (e.g., flood events) or varve counting. The term "varve" (Swedish: layer) was first introduced by De Geer (1912) for outcrops with proglacial sediments and describes finely laminated sediment structures with annual origin. The alternating pale and dark layers are driven by seasonal changes in temperature and precipitation that cause different chemical and biological processes within the lake and its catchment area. When anoxic conditions at the sediment-water-interface are given at least seasonally, i.e. no bioturbation destroys laminations, varves are preserved and provide high-resolution and precise chronologies in calendar years (Zolitschka et al., 2015; Lamoureux, 2001).

Until the 1980s, varve chronologies were the only option for calendar-year chronologies ~~for~~ of sediment records, while AMS radiocarbon dating was still in its infancy and calibration of radiocarbon ages was restricted to tree rings of the Middle and Late Holocene, if at all applied (Pearson et al., 1977; Olsson, 1986). First reviews about methodological advances in the study of annually laminated sediments appeared at the same time (Anderson and Dean, 1988; O'Sullivan, 1983; Saarnisto, 1986) and first long and varve-dated reconstructions were published for Elk Lake, USA (Dean et al., 1984) and Lake Valkiajärvi, Finland (Saarnisto, 1985).

71 Meerfelder Maar and Holzmaar were the first varve-dated lacustrine records covering the entire
72 Holocene and the Late Glacial for Central Europe (Zolitschka, 1989, 1988), followed by records
73 concentrating on the Late Glacial to Holocene transition at Soppensee, Switzerland (Lotter, 1991)
74 and at Lake Gosciaz, Poland (Goslar et al., 1993). As such, the Holzmaar record became one of the
75 best studied lacustrine records in Europe, if not world-wide.

76 To produce the chronology for HZM19 we test and compare different methods integrating varve
77 counts with radiometric measurements using Bayesian age-depth modelling. The advantage of
78 any modelling approach is that all possible calendar ages of calibrated radiocarbon dates and their
79 probability density functions (PDFs) will be tested by using a repeated random sampling method
80 (Blaauw, 2010; Telford et al., 2004). In addition, using the Bayes theorem allows to incorporate
81 information of the accumulation history known prior to modelling. Thus, calendar ages, which are
82 monotonic with depth and with positive accumulation rates in yr cm^{-1} (in sedimentological terms,
83 accumulation rates as they are used for Bayesian age-depth modelling are equivalent to
84 "sedimentation rates", as corroborated by the units used) are calculated (Lacourse and Gajewski,
85 2020; Trachsel and Telford, 2017). This is different and an advantage if compared to the "CLassical
86 Age-depth Modelling" carried out by CLAM (Blaauw, 2010).

87 Currently established programs that use Bayesian statistics are Oxcal (Bronk Ramsey, 2008),
88 BChron (Haslett and Parnell, 2008) and Bacon (Blaauw and Christen, 2011), all of which differ in
89 terms of parameter settings and handling of outliers. In this study, we focus on varve-counting
90 integration methods using Bacon (rBacon version 2.5.7; Blaauw et al., 2021; Blaauw and Christen,
91 2011) for the R programming language (version 4.1.1; R Core Team, 2021), as it is one of the most
92 often used software package in paleo studies and provides many different ways for of
93 implementing additional information. Bacon uses a Markov Chain Monte Carlo (MCMC) sampling
94 strategy to model the accumulation history piecewise using a gamma autoregressive semi-
95 parametric model (Blaauw and Christen, 2011). The accumulation rate of each segment depends
96 on the accumulation rate of the previous segment. Dates are treated using a student's t-
97 distribution. Although Bacon provides default values, the accumulation rate is controlled by two
98 adjustable prior distributions (prior model), the accumulation rate as a gamma distribution and
99 the memory, which describes the dependence of accumulation rates between neighbouring
100 depths as a beta distribution. Both latter parameters are defined by a shape and a strength prior,
101 respectively, in addition to a mean prior. Furthermore, we make use of the number of segments
102 (thick-parameter) recommended by Bacon. The program also allows to incorporate information
103 about hiati and slump events in the profile.

104 We concentrate on approaches using the Bacon package for the R statistical programming
105 software (Blaauw and Christen, 2011), whereas literature also provides comparable methods for

alternative Bayesian age-depth modelling software, such as OxCal (Martin-Puertas et al., 2021; Bronk Ramsey, 2008; Vandergoes et al., 2018), which was also used to integrate varve counting and radiometric dating for the Holocene sediment record HZM96-4a,4b from Holzmaar (Prasad and Baier, 2014). As Bacon provides many different options to incorporate information into the age-depth model, in the literature only few approaches are provided integrating varve and radiocarbon ages (Bonk et al., 2021; Vandergoes et al., 2018; Shanahan et al., 2012). For that reason, we summarize these approaches and compare them directly with each other. This will lead to faster decisions for future studies facing a comparable situation. As Bacon provides many different possibilities to incorporate information in the model, literature provides not many but few very different approaches to integrate varve and radiocarbon ages. For that reason, we sum up those approaches in this study and compare them directly which each other. This might lead to faster decision making for future researchers facing a similar situation.

Since the first coring campaign in 1984, several sediment records have been recovered from Holzmaar and numerous studies were carried out with sedimentological, biological, geochemical and geophysical methods (e.g. Zolitschka, 1989; Lottermoser et al., 1993; Hajdas et al., 1995; Raubitschek et al., 1999; Leroy et al., 2000). However, the early sediment records from Holzmaar, although counted and corrected multiple times, still contain sections of high counting uncertainty and thus suffer from optimal core correlation as it is possible today by applying high-resolution scanning techniques and digital line-scan images. Moreover, independent time control of varve chronologies with AMS radiocarbon dating became available only in the 1990s (Hajdas-Skowronek, 1993), while Bayesian age-depth modelling established as a tool for optimizing dating efforts only during the last decade (Ramsey, 2009) and sediment scanning revolutionized limnogeology and paleolimnology over the last 20 years. Therefore, we revisited Holzmaar to obtain fresh sediment cores for the conduction of innovative and high-resolution (sub-millimetre-scale) sediment scanning techniques to be based on an improved age-depth model.

As chronologies are always a "running target", especially as new scientific methods and approaches appear, it is no wonder that the varve chronology for Holzmaar sediments has developed from its first attempt as "Varve Time 1990" (VT-90) (Zolitschka, 1990) to VT-99 ten years later (Zolitschka et al., 2000). In the course of applying ultra-high (sub-mm-scaled) resolution scanning techniques to athe new set of sediment cores from Holzmaar (HZM19), VT-99 wasis transferred to HZM19 making use of marker layers and radiocarbon ages for correlation as well as of Bayesian age-depth modelling for the creation of an updated varve chronology (VT-22).

Different to earlier studies, we make use of available radiocarbon dates from Holzmaar not only to correct the varve chronology but to combine it with the independent radiocarbon chronology

141 using Bayesian modelling. This integration approach is not commonly used for lacustrine records
142 yet. Here we select three different methods to integrate varve and radiometric dating and apply it
143 to the Holzmaar data. We concentrate on approaches using the Bacon package for the R statistical
144 programming software (Blaauw and Christen, 2011), whereas literature also provides
145 comparable methods for alternative Bayesian age-depth modelling software, such as OxCal
146 (Martin-Puertas et al., 2021; Ramsey, 2008; Vandergoes et al., 2018), which was also used to
147 integrate varve counting and radiometric dating for the Holocene sediment record HZM96-4a,4b
148 from Holzmaar (Prasad and Baier, 2014).

149 In this study we discuss the possibilities to integrate and improve different chronologies by
150 combining a varve chronology with modelling approaches. This is accomplished by testing and
151 comparing integration methods with regard to accuracy and precision from the interpolated varve
152 chronology itself and for a Bayesian model without any varve information. With this integration
153 of all age information we produce the most reliable age estimations for the HZM19 record: VT-22.
154 Based on the best model outcome, this master chronology serves as the chronological base for
155 ongoing and future biological, geochemical and geophysical investigations conducted on the new
156 Holzmaar sediment cores (e.g. García et al., 2022).

157 The aim of our study is to transfer and optimize the existing varve chronology from HZM-B/C to
158 the new sediment record HZM19. In addition, we offer an overview about different approaches
159 for age-depth modelling and their effects on model outcomes to researchers who face comparable
160 challenges, thus supporting their decision making.

161 For this reason, we discuss the possibilities of integrating and improving the chronology by
162 combining the varve chronology with modelling approaches using Bacon. This is accomplished by
163 testing and comparing integration methods with regard to accuracy and precision obtained from
164 the interpolated varve chronology itself and from a Bayesian model without any varve
165 information relying on radiocarbon dates only.

166 With this integration of all age information we produce the most reliable age estimations for the
167 HZM19 record: VT-22. Based on the best model approach, this master chronology of VT-22 serves
168 as the chronological backbone for ongoing and future biological, geochemical and geophysical
169 investigations conducted with the new Holzmaar sediment cores (e.g. García et al., 2022).

2. ~~Materials and Methods~~Regional settings and the Holzmaar sediment record

2.1 Regional ~~s~~Settings

The late Quaternary volcanic maar lake Holzmaar (425 m a.s.l., 50°7'8'' N, 6°52' 45'' E) is located in the western central part of the Rhenish Massif in the West-Eifel Volcanic Field (WEVF; Rhineland-Palatinate, Germany, Fig. 1). The WEVF consists of more than one hundred volcanic cones and maars, of which only nine are water-filled today (Meyer, 2013; Schmincke, 2014). The volcanism in the Eifel region was caused by uplift of the Rhenish Shield since 700 - 800 ka, which started in the NW near Ormont (Meyer and Stets, 2002; Schmincke, 2007). Volcanic activities reached a peak at ca 600 – 450 ka in the central WEVF and then decreased towards Bad Bertrich in the SE (Schmincke, 2007). The uplift is responsible for many eruptive centres at NW-SE trending tectonic faults, along which several phreatomagmatic maar explosions occurred (Büchel, 1993; Lorenz, 1984; Lorenz et al., 2020; Meyer, 1985). One of these eruptions formed the Holzmaar system ca. 40 - 70 ka ago (Büchel, 1993) consisting of three maars with the maar lake of Holzmaar, the raised bog of Dürres Maar and the dry Hetsche or Hitsche Maar (from SE to NW). With 100 m in diameter, the latter is the smallest maar of the WEVF (Fig. 1).

The catchment area of Holzmaar (2.06 km^2) includes the Sammetbach, a creek that flows in and out of the lake. Due to the low erosive energy of the stream no delta formed in the lake (Scharf, 1987; Zolitschka, 1998a). The geology in the catchment area consists of Devonian metamorphic slates, greywackes and quartzites as well as Quaternary loess and volcanic rocks related to eruptions of the Holzmaar system (Meyer, 2013). Holzmaar is located within a conservation area since 1975 protecting the surrounding beech forest (F*agus sylvatica* L.), while ca. 60% of the catchment area is in agricultural use (Kienel et al., 2005).

The lake of Holzmaar has a diameter of 300 m (water surface: 58,000 m^2) and with a maximum water depth of 19-20 m shows a deep and steep-sided morphology typical for maar lakes. Only a small and shallow embayment in the SW interrupts the nearly circular and 1100 m long shoreline. This appendix-like bay developed due to an artificial damming in the late Middle Ages, which was constructed to supply a downstream water mill (Zolitschka, 1998a). For the last glacial, paleolimnological investigations indicate oligotrophic conditions, but eutrophication started already at the onset of the Late Glacial (García et al., 2022). During the Holocene, water quality is affected by human activities, which started during the Neolithic (around 6500 cal. BP) according to pollen analysis (Litt et al., 2009). Together with the inflow of the Sammetbach this caused a steady but slow process of eutrophication and today leads to meso- to eutrophic conditions (Lücke et al., 2003; Scharf and Oehms, 1992; Zolitschka, 1990). The lake is holo- and dimictic with an

204 anoxic hypolimnion during summer stratification (Scharf and Oehms, 1992). Altogether, this
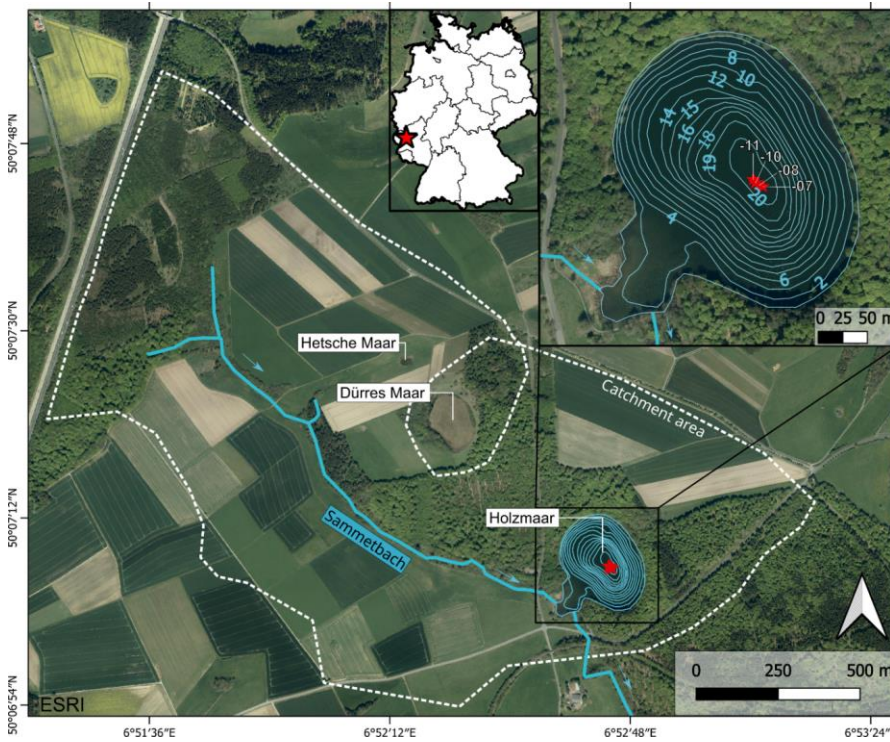205 caused a high potential for varves to be formed and preserved.

206

207 *Figure 1: ESRI Satellite image of the Holzmaar volcanic system and its catchment area (indicated by a white dashed line)*
208 *with Holzmaar, Dürres Maar, Hetsche Maar and Sammetbach (blue line, flow direction indicated by arrows). Upper left*
209 *insert: Location of Holzmaar in Germany (red star). Upper right insert: Bathymetric map with isobaths in meter and coring*
210 *locations (HZM19-07, -08, -10 and -11) marked by red stars.*

211 The catchment area of Holzmaar (2.06 km^2) includes the Sammetbach, a creek that flows in and
212 out of the lake. Due to the low erosive energy of the stream no delta formed in the lake (Scharf,
213 1987; Zolitschka, 1998a). The geology in the catchment area consists of Devonian metamorphic
214 slates, greywackes and quartzites as well as Quaternary loess and volcanic rocks related to
215 eruptions of the Holzmaar system (Meyer, 2013). Holzmaar is located within a conservation area
216 since 1975 protecting the surrounding beech forest (*Fagus sylvatica* L.), while ca. 60% of the
217 catchment area is in agricultural use (Kienel et al., 2005).

218 Holzmaar has a diameter of 300 m (water surface: 58,000 m^2) and with a maximum water depth
219 of 19-20 m shows a deep and steep-sided morphology typical for maar lakes. Only a small and
220 shallow embayment in the SW interrupts the nearly circular and 1100 m long shoreline. This
221 appendix-like bay developed due to an artificial damming in the late Middle Ages, which was

8

3.12.2   Holzmaar lLithology

The four parallel cores HZM19-07, -08, -10 and -11 were aligned and correlated to form the composite profile HZM19 (Fig. 2), which includes 24 core sections and reaches to a basal depth of 14.64 m (Table A3). One technical sediment gap exists at a composite depth of 10.90 m. To determine the precise length of this gap, we use core photographies from a previous Holzmaar core (HZM90-H5u) and determined the technical gap with a length of 12.9 cm (Fig. A1).

In 2019 new sediment cores have been retrieved from Holzmaar to compile the new record HZM19 (see chapter 3.1, Fig. 2). The lithological description of HZM19 follows the characterization of Zolitschka (1998a, 1998b), dividing the HZM84-B/C profile into 12 lithozones (H1 – H12). We added the sediment colours found in HZM19 to this description.

Except H1, all lithozones cover finely-laminated diatomaceous gyttja with varying minerogenic and organic content and as well as colour. All lithozone depths are summarized in Table A14. The transition from light greenish grey (10Y 8/1) and greyish brown (2.5Y 5/2) minerogenic, finely laminated, weakly carbonaceous silts and clays in H1 (12.9 – 14.6 m) to carbonaceous laminated gyttja in light olive brown (2.5Y 5/3), black (10YR 2/1) and light-yellow brown (2.5Y 6/3) with slightly higher organic content in H2 (11.3 – 12.9 m) indicates the transition from the Pleniglacial to the Late Glacial (Fig. 2).

Within H2, the distinct and almost 20 cm thick coarse-grained tephra from the Laacher See eruption (LST, 11.5 – 11.7 m) is deposited, a well-dated isochrone (Reinig et al., 2021) of European lake sediments (Fig. 2). The following lithozone H3 (10.9 – 11.3 m) shows a high minerogenic content and almost no organic components with colours of light greenish grey (5GY 7/1) and grey brown (10YR 5/2), representing the YD at the end of the Pleistocene. Unfortunately, almost one third (12.9 cm) of the YD lithozone H3 is missing due to a technical gap (Fig. 2).

The Holocene sediment shows a periodic change from sections with higher organic content in black (2.5Y 2.5/1) and light olive brown (2.5Y 5/3) (H4: 10.7 – 10.9 m, H6: 9.9 – 10.0 m) to sections

9

with high organic and clastic content in slightly brighter colours like grey (10YR 5/1) (H5: 10.0 – 10.7 m, H7: 9.3 – 9.9 m). The tephra of the Ulmener Maar eruption (UMT, ca. 3 mm thick) occurs in H5 at 10.24 m. The longest lithozone H8 (5.5 – 9.3 m) contains distinctly varved dark reddish brown (5YR 3/2) sediments with high organic content changing towards the top to very dark greyish brown (10YR 3/2) and brown (10YR 4/3) with several up to 5 mm thick lenses of authigenic vivianite. Also, a low carbonate content was recognized. Furthermore, turbidites are observed more frequently from H8 to the top of HZM19 (Fig. 2).

Above H8, the clastic content increases and brightens up to light olive brown (2.5 Y 5/3) and greyish brown (2.5Y 5/2) hues in H9 (4.3 – 5.5 m). In H10 (3.1 – 4.3 m) colours change to darker hues, e.g. olive grey (5Y 4/2) and black (5Y 2.5/2), while the organic content remains high and terrestrial macrofossils like pieces of wood or leave remains occur more frequently towards the top. The organic content is decreasing slightly in H11 (1.1 – 3.1 m), which also contains clastic components and terrestrial plant material as well as turbidites with paler colours, e.g. olive brown (2.5Y 5/3) and grey (2.5Y 5/1). The uppermost lithozone H12 (1.1 m to the top of HZM19) shows unconsolidated organic sediment with a homogenous blackish (5Y 2.5/1) colour for the lower part and brighter dark olive grey (5Y 3/2) sediment at the very top (Fig. 2).

2.3 Evolution of the Holzmaar varve chronologyPrevious Holzmaar chronology

First varve counts and documentation of the annual origin for the finely laminated sediments preserved in the Holzmaar record were carried out in the late 1980's (Zolitschka, 1990, 1991, 1992), presenting the initial Holocene and Late Glacial varve chronology VT-90. Varve Time (VT) refers to varve (calendar) years before 1950 CE (Common Era), which is equivalent to the commonly used reference timescale for radiocarbon dates provided in cal. BP (calibrated years before present, i.e. 1950 CE). The chronology of VT-90 was elaborated for the HZM84-B/C composite record recovered in 1984 and was counted back to the onset of the Late Glacial, i.e. to 12,794 VT-90. This varve chronology was subsequently extended by counting the deeper, periglacial section back to the Last Glacial Maximum, i.e. to an age of 22,500 VT-90 (Brauer, 1994; Brauer et al., 1994).

By including the new sediment cores of HZM90-E/-F/-H, VT-90 was modified resulting in VT-94. These overlapping sediment-core series as well as all other mentioned cores have been recovered from the deepest part of Holzmaar, i.e. from within the 20-m isobath (Fig. 1). This recounting revealed an underestimation of the youngest 5000 years, for which 555 years have been added. This initial underestimation was mainly caused by sections with very thin varves difficult to count (Zolitschka, 1998b). Another discrepancy occurred within the sediments of the Younger Dryas (YD), for which 245 years had to be added. Altogether, the difference from VT-90 to VT-94

10

comprises an addition of 800 years, shifting the basal age of the Late Glacial back to 13,594 VT-94 (Zolitschka, 1998b).

To crosscheck the varve chronology with an independent dating method, 41 samples of terrestrial macrofossils along the entire profile (Tab. A2) have been analysed using the AMS (Accelerator Mass Spectrometryctroscopy) radiocarbon method (Hajdas et al., 1995 and one unpublished radiocarbon date). A comparison between VT-94 and the calibrated radiocarbon chronology shows a discrepancy of +346 years between 3500 and 4500 VT-94 (Hajdas et al., 1995; Hajdas-Skowronek, 1993). This correction factor was estimated by Chi^2-minimization and added by linear interpolation between 3500 and 4500 VT-94. The outcome was VT-95, which consists of three segments. Segment I is covered by an "absolute" chronology until 3500 VT-95, while segment II (3500 - 4846 VT-95) was extended based on the discrepancy detected between varve and calibrated radiocarbon chronologies. Segment III covers sediments from 4846 – 13,940 VT-95 and is considered as a floating chronology (Hajdas et al., 1995; Zolitschka, 1998b).

In 1996 new sediment cores (HZM96-4a, -4b) have been obtained from Holzmaar and VT-95 was transferred to this new record using 26 distinct marker layers with their related VT and error. The age-depth model was subsequently obtained by linear interpolation (Baier et al., 2004). At the same time, novel varve counts for the Meerfelder Maar sediment record established 1880 varve years between the two isochrones of Laacher See Tephra (LST, eruption ca 40 km NE from Holzmaar) and Ulmener Maar Tephra (UMT, eruption ca 13 km NE from Holzmaar) (Brauer et al., 1999), which both are also archived in the Holzmaar sediment record. However, this well-constrained time interval was only 1560 years long for the Holzmaar record. The obviously missing 320 years have been positioned and added to VT-95 based on pollen data from Holzmaar (Leroy et al., 2000), assuming a hiatus for the middle part of the YD biozone at 12,025 VT-95. This resulteds in the latest version (VT-99) of the Holzmaar varve chronology (Zolitschka et al., 2000) with a basal age of 14,260 VT-99 for the Late Glacial.

Varve quality and error estimations were first discussed and described based on multiple counts of selected and representative thin sections (Zolitschka, 1991). Later, different varve quality classes have been described in more detail for VT-90 (Zolitschka et al., 1992) and for VT-95 (Zolitschka, 1998b) with error estimations in the 1σ range (Table A1). Similar error margins were confirmed by counting more recent sediment profiles (HZM96-4a, 4b) from Holzmaar (Prasad and Baier, 2014). In this study, the uppermost part was discussed as showing even higher counting uncertainties. However, no alternative error margins werecan be provided for this section. Thus, we use the data of Table A1 for further evaluations.

3. Materials and Methods

~~2.2~~ 3.1 Sediment core collection

In August 2019, Holzmaar was revisited and four parallel cores (HZM19-07, HZM19-08, HZM19-10, HZM19-11) have been retrieved from the centre of the lake in 19 m water depth (Fig. 1) using a UWITEC piston-corer with ~~a~~ diameters of 90 mm (HZM19-07, -08, -10) and 60 mm (HZM19-11) from a coring platform. The coring locations are distributed evenly along a 12 m-long transect with 4 to 4.4 m distance between coring locations. The recovered sediment cores have lengths of 2 m (HZM19-07, -08, -10) and 3 m (HZM19-11), which have been split in the field into 1 and 1.5 m-long sections, respectively. In total, HZM19-07 covers a sediment depth of 15.5 m (0-15.5 m), while the other sites provided different depth ranges: HZM19-08 (0.25 – 10 m), HZM19-10 (4 – 14 m) and HZM19-11 (1 – 19 m). The water-sediment interface was perfectly recovered with HZM19-07-01 as the piston stopped 15 cm above the sediment surface. At the GEOPOLAR lab (University of Bremen) the cores have been split in halves lengthwise, photographed and visually described using a Munsell colour chart and according to the description guide~~line~~ by Schnurrenberger et al. (2003). Cross correlation of all sediment-core sections was conducted macroscopically using 48 distinct layers (Table A3).

The four parallel cores HZM19-07, -08, -10 and -11 were aligned and correlated to form the composite profile HZM19 (Fig. 2), which includes 24 core sections and reaches to a basal depth of 14.64 m (Table A4~~3~~). One technical sediment gap exists at a composite depth of 10.90 m. To determine the precise length of this gap, we use core photographies from a previous Holzmaar core (HZM90-H5u) and determined the technical gap ~~with~~ to have a length of 12.9 cm (Fig. A1).
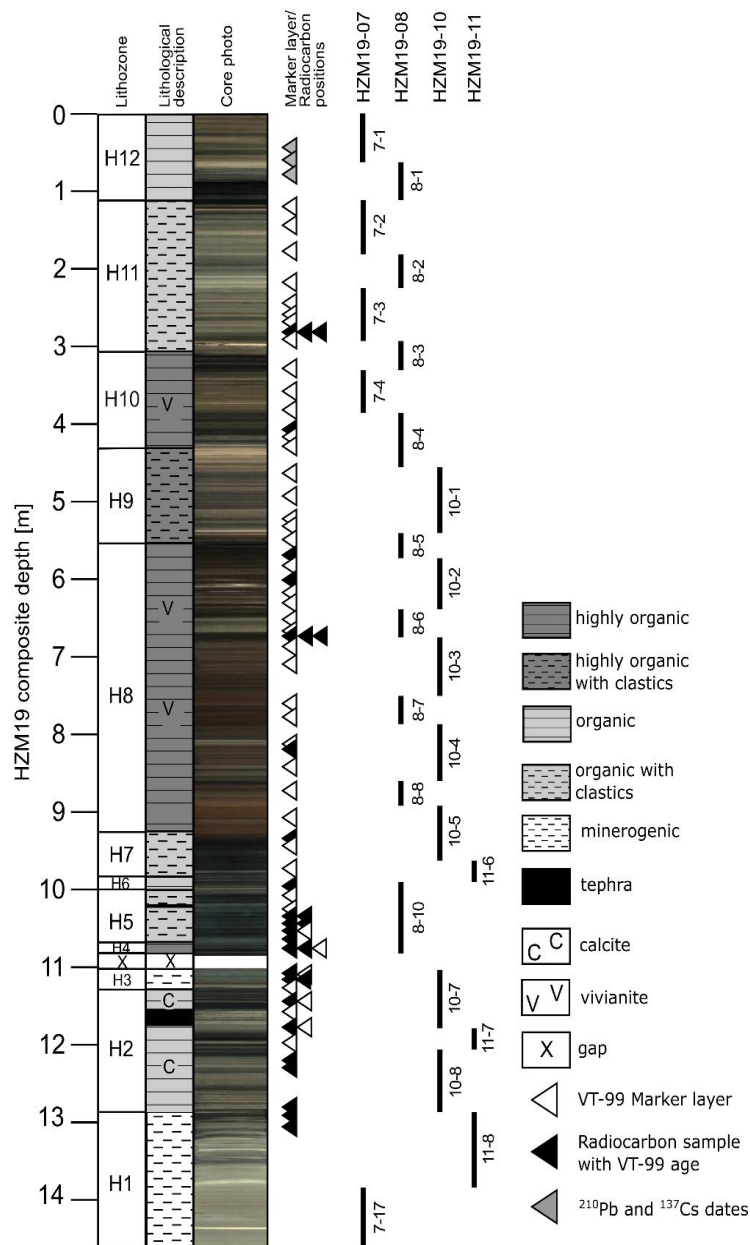
Figure 2: Composite profile of HZM19 with (from left to right) lithozones H1 to H12 (cf., Table A14), lithological description, core photographies taken immediately after core splitting, positions of marker layers and radiometric samples (cf., Tables A52, A75) and core sections used for the composite profile (cf., Table A43).

13

2.3 3.2 Chronology

2.3.1 3.2.1 Evolution of the Holzmaar varve chronology

First varve counts and documentation of the annual origin for the finely laminated sediments preserved in the Holzmaar record were carried out in the late 1980's (Zolitschka, 1990, 1991, 1992), presenting the initial Holocene and Late Glacial varve chronology VT-90. Varve Time (VT) refers to varve (calendar) years before 1950 CE (Common Era), which is equivalent to the commonly used reference timescale for radiocarbon dates provided in cal. BP (calibrated years before present, i.e. 1950 CE). The chronology of VT-90 was elaborated for the HZM84-B/C composite record recovered in 1984 and was counted back to the onset of the Late Glacial, i.e. to 12,794 VT-90. This varve chronology was subsequently extended by counting the deeper, periglacial section back to the Last Glacial Maximum, i.e. to an age of 22,500 VT-90 (Brauer, 1994; Brauer et al., 1994).

By including the new sediment cores of HZM90-E/-F/-H, VT-90 was modified resulting in VT-94. These overlapping sediment-core series as well as all other mentioned cores have been recovered from the deepest part of Holzmaar, i.e. from within the 20-m isobath (Fig. 1). This recounting revealed an underestimation of the youngest 5000 years, for which 555 years have been added. This initial underestimation was mainly caused by sections with very thin varves difficult to count (Zolitschka, 1998b). Another discrepancy occurred within the sediments of the Younger Dryas (YD), for which 245 years had to be added. Altogether, the difference from VT-90 to VT-94 comprises an addition of 800 years, shifting the basal age of the Late Glacial back to 13,594 VT-94 (Zolitschka, 1998b).

To crosscheck the varve chronology with an independent dating method, 41 samples of terrestrial macrofossils along the entire profile (Tab. A2) have been analysed using the AMS (Accelerator Mass Spectroscopy) radiocarbon method (Hajdas et al., 1995 and one unpublished radiocarbon date). A comparison between VT-94 and the calibrated radiocarbon chronology shows a discrepancy of +346 years between 2500 and 4500 VT-94 (Hajdas et al., 1995; Hajdas-Skowronek, 1992). This correction factor was estimated by Chi^2 minimization and added by linear interpolation between 2500 and 4500 VT-94. The outcome was VT-95, which consists of three segments. Segment I is covered by an "absolute" chronology until 3500 VT-95, while segment II (3500 – 4846 VT-95) was extended based on the discrepancy detected between varve and calibrated radiocarbon chronologies. Segment III covers sediments from 4846 – 12,940 VT-95 and is considered as a floating chronology (Hajdas et al., 1995, Zolitschka, 1998b).

In 1996 new sediment cores (HZM96-4a, -4b) have been obtained from Holzmaar and VT-95 was transferred to this new record using 26 distinct marker layers with their related VT and error. The age-depth model was subsequently obtained by linear interpolation (Baier et al., 2004). At the same time, novel varve counts for the Meerfelder Maar sediment record established 1880 varve years between the two isochrones of Laacher See Tephra (LST, eruption ca 40 km NE from Holzmaar) and Ulmener Maar Tephra (UMT, eruption ca 13 km NE from Holzmaar) (Brauer et al., 1999), which both are also archived in the Holzmaar sediment record. However, this well-constrained time interval was only 1560 years long for the Holzmaar record. The obviously missing 320 years have been positioned and added to VT-95 based on pollen data from Holzmaar (Leroy et al., 2000), assuming a hiatus for the middle part of the YD biozone at 12,025 VT-95. This results in the latest version (VT-99) of the Holzmaar varve chronology (Zolitschka et al., 2000) with a basal age of 14,260 VT-99 for the Late Glacial.

Varve quality and error estimations were first discussed and described based on multiple counts of selected and representative thin sections (Zolitschka, 1991). Later, different varve quality

~~classes have been described in more detail for VT-90 (Zolitschka et al., 1992) and for VT-95 (Zolitschka, 1998b) with error estimations in the 1σ range (Table A1). Similar error margins were confirmed by counting more recent sediment profiles (HZM96-4a, 4b) from Holzmaar (Prasad and Baier, 2014). In this study, the uppermost part was discussed as showing even higher counting uncertainties. However, no alternative error margins were provided for this section. Thus, we use the data of Table A1 for further evaluations.~~

~~**2.3.2** Transfer of VT-99 to HZM19~~

~~The varve chronology VT-99 (Zolitschka et al., 2000) was transferred to HZM19 by using 43 predefined marker layers and 41 radiocarbon sampling positions analysed by Hajdas et al. (1995, 2000) with their specific VT-99 ages and errors (Tables A1, A2). Both, marker layers and radiocarbon sampling positions have been identified and justified by comparison with documents describing the samples as well as core photographies from previous studies and sediment profiles, such as HZM90-E, -F, -H and HZM96-4a, 4b. All marker layers cover an age range from 141 to 14,158 VT-99. After assignment, the ages of the marker layers have been linearly interpolated and cumulative counting errors were calculated based on the 1σ errors provided with Table A1.~~

2.3.3 Pb-210 and Cs-137 dating

The isotopes Pb-210 and Cs-137 have been used to radiometrically date the uppermost part of HZM19 at the University of Gdansk. In total, 61 samples were taken with a thickness of 2 cm. The activity of Cs-137 was determined directly by gamma-ray spectrometry from freeze-dried and homogenized samples. Gamma measurements were carried out using a HPGe well-type detector (GCW 2021) with a relative efficiency of 27% and full width at half maximum (FWHM) of 1.9 at the energy of 1333 keV (Canberra). Energy and efficiency calibration were done using reference material CBSS-2 (Eurostandard CZ) in the same measurement geometry like the samples. The counting time for each sediment sample was 24 hours.

Activity of total Pb-210 was determined indirectly by measuring Po-210 using alpha spectrometry. Dry and homogenized sediment samples of 0.2 g were spiked with a Po-209 yield tracer and digested with concentrated HNO_3, $HClO_4$ and HF at a temperature of 100 °C using a CEM Mars 6 microwave digestion system. The solution obtained was evaporated with 6M HCl to dryness and then dissolved in 0.5M HCl. Polonium isotopes were spontaneously deposited within four hours on silver discs. Activities were measured using a 7200-04 APEX Alpha Analyst integrated alpha-spectroscopy system (Canberra) equipped with PIPS A450-18AM detectors. Samples were counted for 24 hours. A certified mixed alpha source (U-234, U-238, Pu-239 and Am-241; SRS 73833-121, Analytics, Atlanta, USA) was used to check the detector counting efficiencies.

~~2.3.4~~ 3.2.2 Bayesian age-depth modelling

~~To produce the chronology for HZM19 we test and compare different methods integrating varve counts with radiometric measurements using Bayesian age-depth modelling. The advantage of any modelling approach is that all possible calendar ages of calibrated radiocarbon dates and their probability density functions (PDFs) will be tested by using a repeated random sampling method (Blaauw, 2010; Telford et al., 2004). In addition, using the Bayes theorem allows to incorporate information of the accumulation history known prior to modelling. Thus, calendar ages, which are monotonic with depth and with positive accumulation rates in yr cm⁻¹ (in sedimentological terms, accumulation rates as they are used for Bayesian age-depth modelling are equivalent to "sedimentation rates", as corroborated by the units used) are calculated (Lacourse and Gajewski, 2020; Trachsel and Telford, 2017). This is different if compared to the "CLassical Age-depth Modelling" carried out by CLAM (Blaauw, 2010).~~

~~Currently established programs that use Bayesian statistics are Oxcal (Ramsey, 2009), BChron (Haslett and Parnell, 2008) and Bacon (Blaauw and Christen, 2011), all of which differ in terms of parameter settings and handling of outliers. In this study, we focus on varve counting integration methods using Bacon (rBacon version 2.5.7; Blaauw et al., 2021; Blaauw and Christen, 2011) for the R programming language (version 4.1.1; R Core Team, 2021). Bacon uses a Markov Chain Monte Carlo (MCMC) sampling strategy to model the accumulation history piecewise using a gamma autoregressive semi-parametric model (Blaauw and Christen, 2011). The accumulation rate of each segment depends on the accumulation rate of the previous segment. Dates are treated using a student's t-distribution. Although Bacon provides default values, the accumulation rate is controlled by two adjustable prior distributions (prior model), the accumulation rate as a gamma distribution and the memory, which describes the dependence of accumulation rates between neighbouring depths as a beta distribution. Both latter parameters are defined by a shape and a strength prior, respectively, in addition to a mean prior. Furthermore, we make use of the number of segments (thick-parameter) recommended by Bacon. The program also allows to incorporate information about hiati and slump events in the profile.~~

Only few studies use the Bayesian approach that integrates varve counting information with radiocarbon dates (Bonk et al., 2021; Vandergoes et al., 2018; Shanahan et al., 2012; Fortin et al., 2019). We extracted three different methods and for comparison include one model only with radiocarbon data, i.e. excluding any VT-99 information. Thus, four different age-depth models (A-D) are compared and discussed:

A) Model based only on radiocarbon dates.

B) This parameter-based varve integration method introduced by Vandergoes et al. (2018) compares several varve integration techniques for sediments from Lake Ohau (New Zealand)

16

using both OxCal and Bacon. Here, we select the integration approach with Bacon, where the "varve counts function" is the source for the prior-parameter of mean accumulation rate. Major changes in accumulation history recorded by the varve data are derived by using the R package "segmented" (Muggeo, 2022). It dissects the sediment sequence and for each resulting segment an individual mean accumulation-rate prior is defined.

C) The tie point-based integration used by Shanahan et al. (2012) integrates the varve chronology from Lake Bosumtwi (Ghana) based on certain tie points with normally distributed age uncertainties of the cumulative error. They address the problem of integrating all individual varve counts, as they cannot be considered as independent chronological datapoints. Thus, they would be weighted too strongly in the model. The compromise we have chosen for this study, is placing one varve tie-point every 100 years. As there is no varve counting available for HZM19 but VT-99 ages based on marker layers, we implement them with cumulative errors as tie points instead.

D) The segmented and parameter-based integration introduced by Bonk et al. (2021) provides the most complex method for varve integration. The problem of not or poorly varved sections in the sediment profile of Lake Gosciaz (Poland) is compensated by dividing the profile into three sections and interpolating the section with low-quality varves using Bayesian modelling. For the Holzmaar record, we define four sections: sections 2 and 4 are based on Bayesian modelling, while sections 1 and 3 rely on VT-99. Section 3 is treated as a floating chronology and placed based on the sum of calibrated radiocarbon probabilities lying within this section. To tighten the two Bayesian modelled sections to the following varved sections, an anchor tie-point based on the oldest age of the younger sections is implemented.

For each model we use ~~of~~ radiocarbon dates published by Hajdas et al., 1995 and Hajdas et al., 2000 (Table 5), the calibration curve IntCal20 (Reimer et al., 2020) and make use of the default accumulation strength and memory priors. We also implement a surface age of -69 ±~+~ 1 cal. BP as tie point with a normal distributed error to anchor the chronology to present-day.

4. Results and Interpretation

4.1 Transfer of VT-99 to HZM19

The varve chronology VT-99 (Zolitschka et al., 2000) was transferred to HZM19 by using 43 predefined marker layers and 41 radiocarbon sampling positions analysed by Hajdas et al. (1995, 2000) (Fig. A2) with their specific VT-99 ages and errors (Tables A2~1~, A5~2~). Both, marker layers and radiocarbon sampling positions have been identified and justified by comparison with documents describing the samples as well as core photographies from previous studies and sediment profiles, such as HZM90-E, -F, -H and HZM96-4a, 4b. All marker layers cover an age range from 141 to 14,158 VT-99. After assignment, the ages of the~se~ marker layers have been linearly

17

interpolated and cumulative counting errors were calculated based on the 1σ errors provided with Table A2~~1~~.

All 84 marker layers distribute in HZM19 from 1.16 - 12.93 m and cover the entire VT-99 age range ~~from 141 to 14,158 VT-99~~ (Table A5~~2~~). During the transfer of marker layers to HZM19 and comparison between HZM19 and previous Holzmaar sediment cores (HZM84-B/C, HZM92-E/-F/-H, HZM96-4a/4b) differences in position of the lowermost marker layers occurred (Fig. ~~ure~~ A2). All records show differences in distances between marker layers (ML) 1 (14,156 VT-99), ML-2 (14,152 VT-99) and ML-3 (13,646 VT-99) making a clear assignment of these layers difficult. Thus, we excluded these three marker layers for the transfer of VT-99 to HZM19. The lowermost applied marker layer is therefore ML-4 with a varve age of 13,087 VT-99 at a depth of 11.86 m. Because of inconsistencies in documentation, we excluded two more VT-99 ages, i.e. those related to the radiocarbon ages HZM-46 and HZM-10.1 (Table A5~~2~~).

The marker layer density reaches a mean value of 5.5 dpm (dates per millennium) being most frequent before 10,000 and after 6000 cal. BP (Fig. 3~~4~~). We use a linear interpolation to receive an age-depth model based only on VT-99 with a resulting accuracy of 282 years as a mean age range and a maximum age range of 744 years (Table A6).

The radiocarbon dating density of HZM reaches an overall mean value of 2.7 dpm (Fig. 3~~4~~), which is 35% higher than the 2 dpm recommended for Bayesian modelling by Blaauw et al. (2018). However, their distribution is uneven. Radiocarbon dates are most frequent for ages >10,000 cal. BP with 3-7 dpm (mean: 5 dpm) (Fig. 3~~4~~). A minimum density of radiocarbon dates (0-1 dpm) is obtained from 10,000-6000 cal. BP (mean: 0.5 dpm). Therefore, a chronology based on the available radiocarbon data within this section should be interpreted with caution. Dating density for the uppermost 6000 years is higher and varies between 1 and 4 dpm (mean: 2.2 dpm).

When we compare VT-99 with radiocarbon ages calibrated with the latest calibration curve IntCal20 (Reimer et al., 2020), an overall agreement with marker layers is observed. Only for the lowermost part below approximately 10.64 m, we observe an increasing underestimation of VT-99 in relation to IntCal20 calibrated radiocarbon ages (Fig. A3~~2~~, Table A5~~2~~). This was already observed by Hajdas et al. (2000) in comparison to Intcal98 but has not been corrected yet.
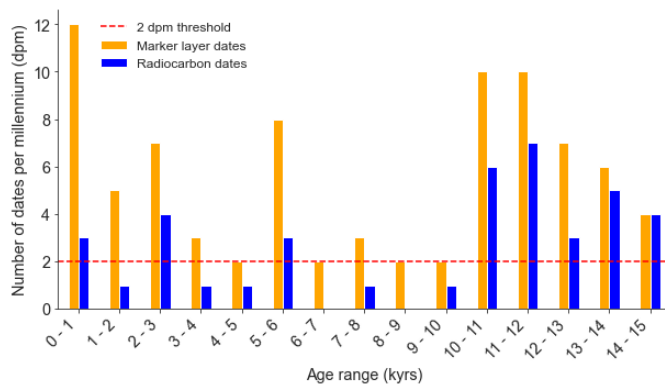
18

531

532

Figure 3: Number of dating points per millennium (dpm) of HZM19 for marker layers (n: 84, mean: 5.5 dpm) and radiocarbon dates (n: 41, mean: 2.7 dpm). Red dotted line marks the recommended threshold of 2 dpm for Bayesian modelling suggested by Blaauw et al. (2018). Surface age and three ages estimated by Cs-137 are excluded.

3.

3.2   4.2 Chronology
New chronological information

3.2.1 4.2.1 Pb-210 and Cs-137 dating

The profile of unsupported Pb-210 activity concentration shows a gradual rather than an exponential decrease within the first meter of HZM19 (Fig. 43). Additionally, a plateau from 8 to 30 cm is interpreted as a section with rapid deposition of homogenous material and will be treated for further analyses as a slump event. Despite this irregularity, the gradual decrease in unsupported Pb-210 activity with depth indicates high sedimentation rates. We use the CFCS (Constant Flux Constant Sedimentation) model to estimate mean sedimentation rates of 1.09±0.13 cm yr^{-1}. This value should be treated with caution but suggests that the uppermost meter (including a 22 cm-thick slump) was deposited in ca. 70 years.
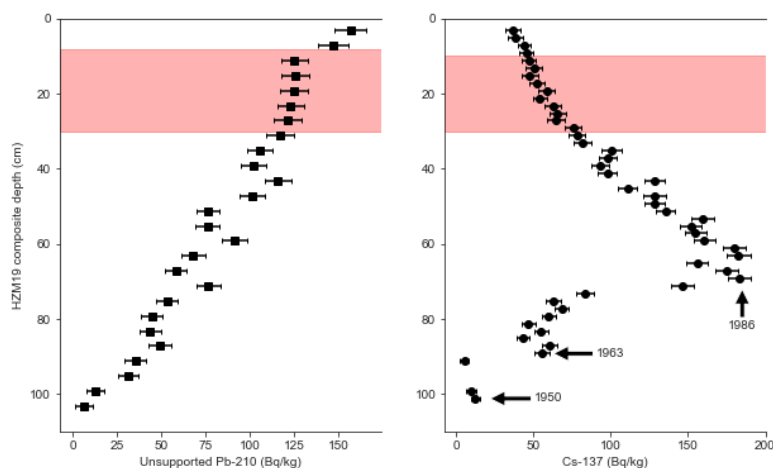
Figure 43: Results of unsupported Pb-210 (left) and Cs-137 (right) measurements with error bars for the uppermost 110 cm of HZM19. Shaded areas indicate the plateau shown by Pb-210 data, black arrows mark peaks assigned to radiochronological events (given numbers are ages in years CE).

The variability of Cs-137 activity concentrations delivers potentially three historical markers (Fig. 4)3). The Cs-137 profile is smooth lacking sharp peaks due to high sedimentation rates and likely sediment focusing. First traces of Cs-137 are recognizable at 101.2 cm and indicate atomic bomb testing in the early 1950's. At 89.2 cm, there is a significant increase signalling atmospheric fallout in the early 1960's in response to peak atomic bomb testing. Finally, at 69.2 cm a strong increase in Cs-137 documents the 1986 Chernobyl accident (Fig. 43, Table A75). This interpretation is generally in line with the results of Pb-210 dating. The shape of the Cs-137 record also corresponds nicely to the results of Sirocko et al. (2013), who measured Cs-137 on sediments from Schalkenmehrener Maar and Ulmener Maar (both WEVF). For both of these cases, the 1986 Chernobyl peak is also much larger than the one related to the start of atomic bomb tests in 1963.

3.2.2   4.3 Age-depth modelling

Four different Bayesian age-depth models are calculated, of which three include varve ages (Model B-D) and one only radiocarbon ages (Model A). In common for all model runs are the default memory priors and the use of the IntCal20 calibration curve (Reimer et al., 2020). Furthermore, based on the Pb-210 and Cs-137 dating analysis, a slump at a composite depth of 8-30 cm was implemented, as well as the LST from 11.52 – 11.71 m. As known from previous varve

Formatiert: Links, Einzug: Links: 0.63 cm, Zeilenabstand: Mehrere 1.08 ze, Keine Aufzählungen oder Nummerierungen

and pollen studies of the Holzmaar record (Brauer et al., 1999; Leroy et al., 2000), 320 years are missing during the YD and have been included into VT-99 at 12,025 VT-99. Based on the study of Leroy et al. (2000), we were able to locate the position of the YD hiatus to a depth of 11.09 m, which we implemented for each model with a maximum duration of 320 years. In addition to marker layers and radiocarbon dates, we included the surface age of -69 ± 1 cal. BP and three events dated by Cs-137 (Table A75).

Preliminary test runs reveal two necessary changes to be made for the calculations: 1) The default number of iterations is too low to produce a robust model for the entire HZM19 sediment sequence. Thus, we use the *Baconvergance()*-function of Bacon to estimate the number of iterations needed. This function repeats the calculations and tests if the MCMC mixing of the core results in a robust model by calculating the "Gelman and Rubin Reduction Factor" (Brooks and Gelman, 1998). Good mixing is indicated by a threshold of <1.05, which in our case was reached after three iterations when the number of iterations was increased to 40,000. This results in a better mix of MCMC iterations but also in long calculation times (> 5 hours). 2) For each test run, Bacon predicted ages consistently too old for the LST, which is probably caused by slightly too old ages of the surrounding radiocarbon dates (Table A52). To gain a better comparability with studies from other sites, we decided to include the latest LST age of 13,006 ± 9 cal. BP (Reinig et al., 2021, Table A75).

In addition, we extended the age-depth model to a maximum depth of 14.64 m, as ongoing analyses exceed the lowermost dated level. However, in the following chapters we only discuss the model output between the first (ML36/1) and the last (HZM-19) marker layer at 12.93 m (Table A52) and compare it with the interpolated varve chronology (VT-99).

After each calculation and if the Bacon output indicates a highly variable log of objectives or MCMC iterations, we made use of the scissor()-command to achieve a better mixing of the output. All Bacon model outputs with their settings and additional information are shown in Figure 5A3 and related ages are listed in Table A6.

The **model without varve integration (Model A)** is based on the year of sediment recovery (surface age), three dates estimated by Cs-137 analyses, the age for the LST (Reinig et al., 2021) and 41 calibrated radiocarbon probability density functions (Fig. 5A3A). Different to Hajdas et al. (1995), this model includes the outlier of HZM-23, but excludes HZM-24 and other described outliers (Table A52).

21
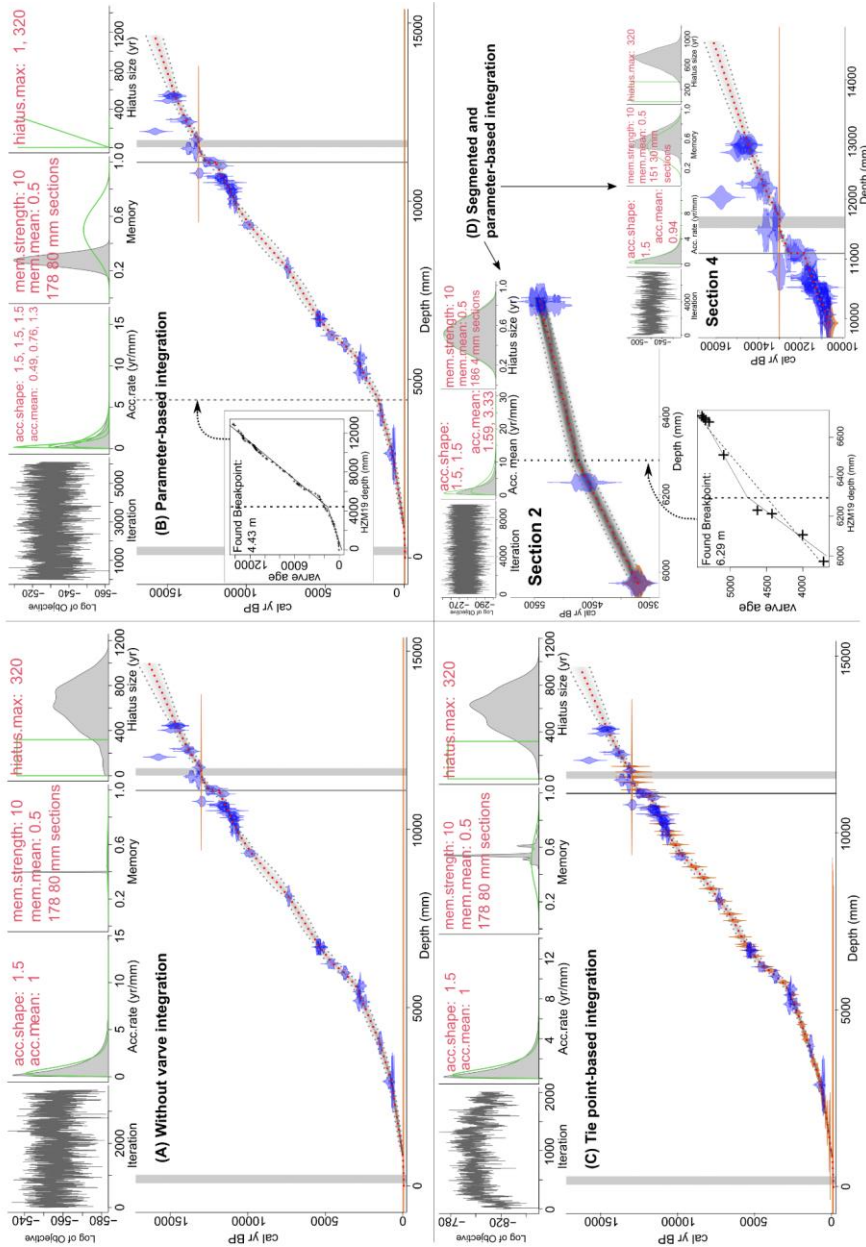
Figure 5: Bacon output for Model A, B, C and D (sections 2 and 4). Each output with indicator panels from top left to right: MCMC iterations, prior (green) and posterior (grey) for accumulation rate distribution, memory and hiatus with defined settings in red. Main panel: model with calibrated radiocarbon date probabilities (blue), tie-points with normal distribution (orange) and the posterior age-depth model with mean (red dotted line) and 95% confidence intervals (gray dotted line). Vertical gray lines (from left to right): slump event, defined hiatus and Laacher See Tephra. In additional panels of Models B and D2 boundaries indicating major changes in accumulation rate are provided as vertical dotted lines.

610

611 Model A results in an age of 14,615 [minimum: 14,339, maximum: 14,926] cal. BP at the
612 lowermost dated depth of 12.93 m with a mean age uncertainty of 468 yrs. The maximum age
613 uncertainty of approx. 1056 years occurs at a depth of 8.86 m within lithozone H8 (Table A6),
614 where radiocarbon dating density is <1 dpm (Fig. 34).

615 The **parameter-based integration (Model B)** integrates VT-99 using all dates as in Model A and
616 adjusts the prior information given for the calculation based on the varve accumulation-history.
617 We follow the procedure presented by Vandergoes et al. (2018) and calculate a breakpoint based
618 on ages and depths of the marker layers at 4.43 m, i.e. at 1312 VT-99 (Fig. 5A3B). This boundary
619 is implemented as an additional hiatus to the Bacon code with a duration of 1 year. The
620 accumulation rate prior is set based on published sedimentation rates (Zolitschka et al., 2000).
621 We calculate with a mean of 0.49 yr/mm for the uppermost part (71-1312 VT-99), with 1.30
622 yr/mm from 1312 to the YD hiatus at 12,025 VT-99 and with 0.76 yr/mm from the YD hiatus to
623 the lowermost age of 14,158 VT-99. Model B is calculated using the same parameters as for Model
624 A and with the same treatment of outliers.

625 The resulting posterior model shows similarities to Model A, having a maximum mean age of
626 14,456 [min.: 14,236, max.: 14,749] cal. BP at a depth of 12.93 m and a mean 95% confidence
627 interval of 456 years with a maximum of 1064 years at 8.78 m, i.e. within the period of lowest
628 radiocarbon dating density (Fig. 34).

629 The **tie point-based integration (Model C)** is based on the approach used by Shanahan et al.
630 (2012). We include 43 marker layers with related VT-99 ages and cumulative errors as normal
631 distributed tie points into the model, which adds to the dates used in Models A and B and sums up
632 to 89 dates. This approach increases the amount of chronological information and fills areas with
633 larger gaps between radiocarbon dates. The model was run with default settings provided by
634 Bacon (Fig. 5A3C). Bacon recognizes the outliers in the same way as by previously described
635 models.

636 Model C results in a maximum age of 14,614 [min.: 14,332, max.: 14,919] cal. BP (at 12.93 m) with
637 a mean 95% confidence interval of 329 years, which is better than for Models A and B. A maximum
638 age range of 749 years is given at a depth of 9.18 m, which is also slightly better than for previously
639 presented models. However, Model C produced MCMC iterations with highest noise and it was
640 difficult to cut out a well-mixed section (Fig. 5A3C, upper left panel).

641 The **segmented and parameter-based integration (Model D)** is a more complex method of
642 varve integration used by Bonk et al. (2021) and was adapted for the HZM19 profile by dividing
643 the varve chronology of VT-99 into four sections. This separation is based on variations of

23

644 counting uncertainty, radiocarbon sampling density and an increasing offset of VT-99 to the latest
645 calibration curve IntCal20 (Fig. A3~~2~~).

646 Section 1 (0 – 5.98 m) and Section 3 (6.70 – 9.90 m) are transferred and interpolated based on VT-
647 99 marker layers, as they are consistent with calibrated radiocarbon data (Section 1) and have
648 well-preserved varves with small counting errors of ±0.7% (Section 3). Section 2 (5.98 – 6.70 m)
649 and Section 4 (9.9 – 14.6 m) are reported as showing higher counting uncertainties (Section 2) or
650 increasing differences between VT-99 and the calibration curve (Section 4). Thus, we replace the
651 varve chronology in Sections 2 and 4 with Bayesian age-depth modelling (Fig. 5A~~3~~D). Section 4
652 also contains very dense radiocarbon dates (Hajdas et al., 2000), which increase the predictability
653 of Bacon (Fig. 3~~4~~).

654 Section 1 is based on linear interpolation for ages of the sediment surface (-69 ± 1 cal. BP), three
655 dates derived by Cs-137 analyses (Table A7~~5~~) and 25 ages of marker layers with a basal age of
656 3704 ± 134 cal. BP at the position of HZM-25 (Table A5~~2~~).

657 The modelled Section 2, previously identified as a section with sedimentation rates >2.86 yr/mm
658 and therefore a source of high counting uncertainties and underestimation of varve ages
659 (Zolitschka et al., 2000), consists of five radiocarbon dates (Table A5~~2~~) and the basal age of Section
660 1 (3704 ± 134 cal. BP) as anchor point for Section 2. To reduce the resulting gap between first and
661 second sections, we reduce the error estimation for the anchor point to ±70 years (±~~+~~0.5σ). As
662 there is a major change in sedimentation rates within this section, we calculated a boundary
663 similar as in Model B using the marker layers of this section (Fig. 5A~~3~~D). This allows defining a
664 boundary at the depth of 6.29 m with adjusted accumulation means of 3.33 yr/mm above (5.98 –
665 6.29 m) and 1.59 yr/mm below (6.29 – 6.70 m), using published sedimentation rate data
666 (Zolitschka et al., 2000). Based on suggestions by the software, the "thick"-parameter was set to 4
667 mm. The resulting model covers and age range from 3709 [min.: 3591, max.: 3825] to 5419 [min.:
668 5329, max.: 5548] cal. BP (Fig. 5A~~3~~D section 2).

669 Section 3 interpolates 16 marker layers (Table A5~~2~~), which are treated as a floating chronology.
670 The placement of the anchor point relates to the basal age of the lowermost calibrated
671 radiocarbon date (HZM-4.3) in Section 2 (Table A5~~2~~) and the maximum sum of the four calibrated
672 radiocarbon PDFs within this part with a summed probability of 0.076 at 5450 ± 165 cal. BP (Fig.
673 A4-A).
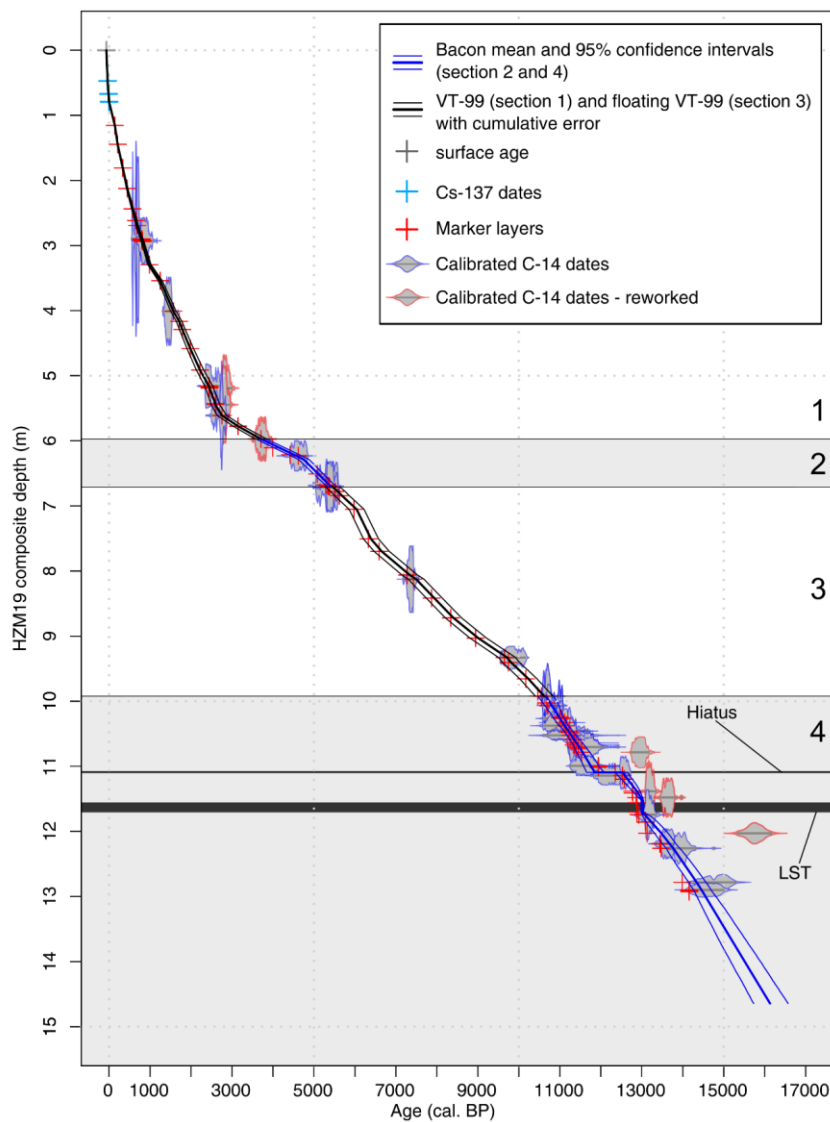
Figure 6: Age-depth model for HZM19 based on Model D with Sections 1 and 3 based on VT-99 (section numbers at the right) and Sections 2 and 4 based on Bayesian modelling (shaded).

In comparison to the original VT-99 this approach results in a shift of +65 years for all marker layers within Section 3 (Fig. A4-B). Thus, a basal age of 10,619 ± 213 cal. BP is obtained for Section 3.

The basal age of Section 3 is implemented as the anchor tie-point for the Bacon calculation of Section 4 with a reduced error of 100 years to tighten both sections closer to each other. In

25

addition to the difficulties based on missing sediment within the YD, this section is the source of highest counting uncertainties for VT-99. Section 4 is based on 25 radiocarbon dates and the latest age estimation for the LST (Table A5~~2~~). As in Section 2, we adjusted the sedimentation rate prior (= 0.94 yr/mm) based on VT-99 accumulation rate data (Zolitschka et al., 2000). The Bacon software suggests a segment length of 30 mm that we applied. The resulting model covers an age range from 10,663 [min.: 10,457, max.: 10,864] to 14,485 [min.: 14,287, max.: 14,721] cal. BP at 12.93 m (Fig. 5A~~3~~D, Section 4).

If all sections are merged, the continuous age-depth relationship forming Model D (Fig. 6~~5~~) consists of 63% VT-99 ages and 37% Bacon modelled ages with in total 80 missing years between the sections, as it is not possible to determine the exact start and end age of the models. This segmented and parameter-based integration model results in a maximum age of 14,485 [min.: 14,287, max.: 14,721] cal. BP (at 12.93 m) with a mean age uncertainty of 229 years, which is the smallest of all four tested models. The maximum age range is 447 years at 11.09 m depth and thus considerably smaller compared to those of Models A to C (Table A6).

~~2.1.1~~ **4.4** Comparison of model output with VT-99

The comparison of all presented models differs in means and accuracies of predicted ages along the core (Fig. 7~~6~~A1; B1; C1; D1), which becomes more evident in comparison with VT-99 (Fig. 7~~6~~A2,3; B2,3; C2,3; D2,3). These differences in mean modelled age and mean VT-99 age vary in direction and amplitude (Fig. 7~~6~~A2; B2; C2; D2). The largest age differences during the Holocene occur in Model A and B with up to 300 years between 4 and 6 m depth (Fig. 7~~6~~A2; B2). The defined boundary in Model B results in large differences within the boundary area, predicting much younger ages than VT-99. Due to the small cumulative counting uncertainty of VT-99 in the upper part of the profile, the mean of Model B outranges the VT-99 error in most sections above 6 m (Fig. 7~~6~~B2).

Formatiert: Einzug: Links: 0.63 cm, Keine Aufzählungen oder Nummerierungen
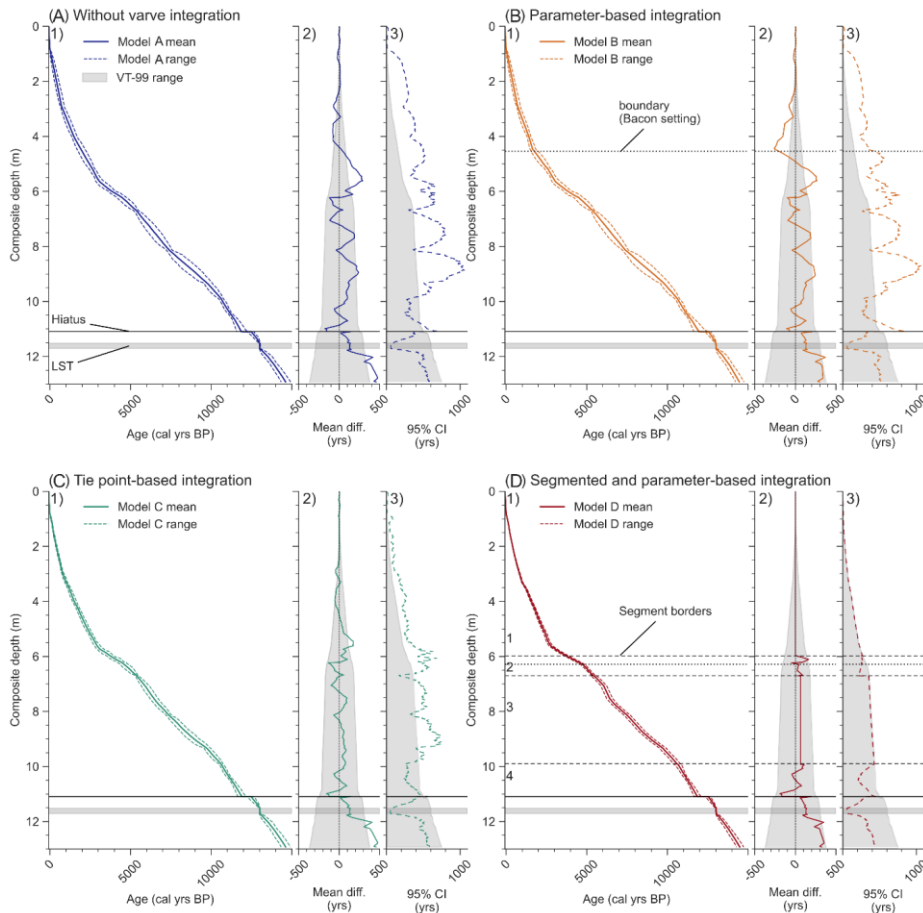
The approach used for Model C reduces the difference between VT-99 and the model, probably a result of increased dating density (Fig. 76C2). This approach also leads to less over- and underestimations of the model's mean age and the VT-99 age range (Fig. 76C2). Only the segmented insertion of VT-99 in model D results in comparable ages during the Holocene (Fig. 76D2)

In the Late Glacial part below 11 m, all models produce ages constantly older than VT-99 (Fig. 76A2, B2, C2, D2). The age differences are even higher (up to 477 years), when the Bacon prior for accumulation rates was not adjusted to VT-99 (Fig. 76A2, C2). In the other cases the maximum age differences are 369 and 354 years for Model B and D, respectively (Fig. 76B2, D2). Hajdas et al. (2000) already observed a shift between the varve ages of radiocarbon dated samples and

27

719   calibrated ages using the INTCAL98 calibration curve (Stuiver et al., 1998) and discuss the
720   difference using the LST age estimation from Meerfelder Maar (12,880 VT). However, no
721   adjustment has been made to fit the VT-99 ages to the calibration curve. With the LST dated to
722   13,006 ± +−9 cal. BP (Reinig et al., 2021) and the use of the INTCAL20 calibration curve, an
723   underestimation of VT-99 compared to the calibration curve is still existing (Fig. A3₂). Therefore,
724   a correction of ages older than 12,800 cal. BP is needed to ensure comparability of HZM19 to other
725   sites.

726   In order to find the best method to transfer VT-99 to HZM19 and to improve the chronology by
727   using Bayesian modelling, a closer look to each model's accuracy is necessary (Fig. 76A3, B3, C3,
728   D3). In comparison to the cumulative VT-99 counting error, Models A and B show maximum
729   differences in age uncertainties up to +655 and +665 years, respectively (Table A6). Especially
730   below 9.82 m, both models predict ages with larger uncertainties than the estimated counting
731   error for VT-99, particularly with increasing distance to radiocarbon dated levels. Therefore, no
732   improvement in accuracy of age estimations is observed when using the parameter-based
733   approach (Model B).

734   The tie point-based Model C also predicts larger uncertainties than VT-99 below 9.82 m (Fig. 76C),
735   whereas the overall difference of the age range is reduced to a mean of 47 years with a maximum
736   of +401 years (Table A6). Only the segmented and parameter-based Model D shows no
737   significantly enlarged age uncertainties and an overall improved mean age range as it adapts the
738   cumulative error of the varve chronology in Sections 1 and 3 (Table A6). The overall improvement
739   occurs in Sections 2 and 4, which is the result of more detailed prior settings for the model run.
740   However, all age models result in more accurate age estimations in the Late Glacial part, where
741   the cumulative counting error is higher and radiocarbon dating sampling is dense. But still we see
742   that Models C and D perform best within this section, as they predict ages with constantly lower
743   uncertainty ranges than VT-99. This is in contrast to the other models, which show increased and
744   therefore larger uncertainties at a depth of ca. 11 m. As we calculate this section in Model D with
745   the same data like for Model A and B, we assume that the better adjustment of the sedimentation
746   rate mean prior of Model D influences the model's accuracy. In terms of accuracy, there are no
747   general improvements in calculating a single model for the entire record, but improvements are
748   realised by adjusting the priors in a more detailed way.

749

~~3.2.3~~ 4.5 Comparison of model output with ~~the~~common isochrones ~~UMT and LST and the YD biozone~~

The tephra layers of UMT and LST have been identified for sediments from Holzmaar and Meerfelder Maar (Brauer et al., 1999). The varve age of 11,000 VT-99 for UMT was derived from the Holzmaar chronology (Zolitschka, 1998b), while the YD hiatus of this site did not allow any calendar-year estimation for LST. As no such hiatus exists between these two isochrones at Meerfelder Maar, the age for the LST was derived as 1880 varve years older than UMT, i.e. as 12,880 VT-99. A recent study presents a new and 126 years older age for the LST (Reinig et al., 2021). This age of 13,006 cal. BP was implemented for the calculation of Models A-D.

When we compare all models, the age estimations for UMT ~~and LST~~ are close to the published ages with the UMT dated ca. 20-50 years earlier and thus matches well within the 95% confidence interval (Fig ~~8~~A5, Table A6). Due to the new age of LST, the distances between both isochrones vary from 2030 (Model D) to 2057 (Model C) years, which is 150-177 years more than counted for Meerfelder Maar (Fig ~~8~~A5).

The main differences occur in prediction of the end of the YD that defines the transition to the Holocene. The rapid cooling and subsequent warming left behind easy to recognize traces in many European lake records increasing the comparability between sites. The entire YD is not covered by HZM19 due to a technical gap. Nevertheless, we are able to estimate depth and time range based on detailed pollen investigations (Leroy et al., 2000). Using VT-99, Leroy et al. (2000) date the onset of the YD, i.e. the Allerød/Younger Dryas transition (AL/YD) to 12,606 VT-99 and the Younger Dryas/Preboreal (YD/PB) transition to 11,632 VT-99 with a 320 years hiatus at 12,025 VT-99. For HZM19 these boundaries occur at 10.88 m (YD/PB), at 11.26 m (AL/YD) and the hiatus at 11.11 m (Fig. ~~7~~6, ~~8~~A5).

All model runs predict a YD duration in the range of 1012 (Model C) to 1073 (Model D) years, which is longer than the 974 years given by VT-99 (Fig. ~~8~~A5, Table A6). However, the predicted times are closer to its duration counted for Meerfelder Maar (1080 years) (Brauer et al., 1999) or the even longer time span~~s~~ detected for Lake Gosciaz (1150 years) (Bonk et al., 2021).~~.~~

Moreover, ~~both~~onset and~~the~~ end of the YD ~~transitions~~ ha~~ve~~s been predicted within the 95% confidence interval comparable to VT-99 (Fig. ~~8~~A5, Table A6) and to the Meerfelder Maar record. Only the AL/YD transition varies between 12,694 (Model C) and 12,737 (Model B) cal. BP and, thus, is predicted earlier than for VT-99 (12,606 VT-99). However, this age range still covers the age estimations from Lake Gosciaz (12,620 [min.: 12,389, max.: 12,753] cal. BP) and Meerfelder Maar (12,680 [min.: 12,640, max.: 12,720] cal. BP) (Fig. ~~8~~A5). In difference, the YD/PB transition varies between 11,655 (Model D) and 11,723 (Model B) cal. BP, which is slightly earlier than

784   estimated by Meerfelder Maar (11,600 [min.: 11,570, max.: 11,630] cal. BP) and much earlier than

785   the age estimation for Lake Gosciaz (11,470 [min.: 11,264, max.: 11,596] cal. BP) (Fig. 8A5). These

786   discrepancies between the boundaries of the YD biozone obtained by VT-99 and those obtained

787   by the model runs are probably related to the new and 126-year older age for the LST, which is

788   included with all models. Thus, age discrepancies are attenuating towards the UMT with 110 years

789   at the AL/YD transition and 57 years at the YD/PB transition (Fig. 8A5).

4.5.   Evaluation of ~~the~~ different varve integration techniques

792   All models predict convincing age estimations for the isochrones of ~~LST and~~ UMT, whereas the

793   prediction of the YD between both isochrones remains somewhat ambiguous, due to a

794   documented hiatus and too few radiocarbon ages being available for this biozone.

795   In terms of accuracy and precision, the varve-integration technique applied in Model D,

796   introduced by Bonk et al. (2021), results in most convincing age estimations for HZM19. Especially

797   in terms of accuracy, none of the completely Bayesian modelled age-depth relationships improved

798   the small age uncertainties of VT-99 in the upper part. Only in sections with markedly higher

799   radiocarbon sampling density or in sections with high varve counting uncertainty the Bacon

800   models perform better and result in more accurate age estimations than VT-99.

801   In comparison, Model B shows nearly no improvement over the approach without varve

802   integration (Model A). The reason is probably the low-resolution definition of sedimentation rate

803   changes (boundaries) for HZM19, which does not reflect the complex accumulation history. Also

804   Vandergoes et al. (2018) reject this integration model. We suggest that this form of varve

805   integration is more useful for less complex and for shorter sediment ~~profiles~~ records.

806   Better results are observed applying Model C, which is actually the easiest to apply. The accuracy

807   is improved compared to Models A and B as the dating density increases significantly. Based on

808   the Bayesian approach, this leads to smaller age ranges as higher uncertainties occur with

809   increasing distances to dated levels. The resulting mean age is more constrained by VT-99. The

810   accuracy might be improved by additional adjustments of the sedimentation-rate prior (here:

811   based on VT-99). However, varve ages inserted as tie points are included with normal distribution.

812   Therefore, they should not be interpreted as independent measurements with not ~~n~~ normally

813   distributed PDFs. Bayesian statistics could weight tie points too much when they are included ~~too~~

814   densely. Therefore, this approach should be interpreted with care.

815   The best result in precision and especially accuracy is achieved by the segmented and parameter-

816   based Model D. This approach is the most challenging, ~~but~~ and makes advantage of both, the high

817 accuracy of varve counting and the Bayesian approach for densely radiocarbon dated sections.
818 The main difference to the other models is that Model D replaces the sections of lower dating
819 accuracy with modelled ages that incorporate varve information and radiocarbon measurements,
820 which result in a much better performance.

821 For upcoming geochemical and geophysical studies of the HZM19 record, we will use Model D. As
822 parts of VT-99 (63%) are included in the new chronology, we will refer to it as chronology "VT-
823 22", which delivers highly accurate age estimations for each depth of the Holocene sediment
824 profile HZM19. Altogether, this will improve the comparability of the Holzmaar record with other
825 sites.

5.6.   Conclusion

827 As limnogeological and varve studies proceed, new techniques for sediment analysis develop.
828 Thus, previous studies can be improved by reinvestigation. However, many of the previously
829 studied sediment cores are not available for analysis anymore. We expect such cases to happen
830 more frequently in the future. Rarely, the rather time-consuming and expensive chronological
831 studies, especially if the counting of varves is involved, will be funded a second time. This
832 increases the need for finding best ways to adapt varve chronologies obtained during previous
833 studies and to transfer them efficiently and precisely to new sediment cores.

834 For the well-dated Holzmaar record, we tested three different approaches for the integration of
835 varve counting and radiocarbon dating using Bayesian modelling and applied them to the new
836 composite profile from Holzmaar (HZM19). We conclude that all models result in accurate and
837 precise age estimations. However, with higher dating density and more prior settings used to
838 adjust the Bacon model runs, the model output is enhanced. This is confirmed by results of Model
839 D, which improved and corrected the age estimations considerably. In contrast, Models B and C
840 show nearly no improvement over compared to VT-99 just like the output of Model A without
841 varve integration.

842 Multiple varve counting is still one of the best approaches of building a reliable chronology for
843 lacustrine sediment archives. However, the occurrence of hiati or errors in varve counts lead to
844 larger uncertainties with increasing depth that need to be corrected by using independent dating
845 techniques. Therefore, if varve and radiocarbon data are available, like it is the case for Holzmaar,
846 the transfer of both to form a new and integrating chronology is the best option.

847 For this study of varve integration, we use Bacon. The parameter adjustment of Bacon is complex
848 and especially beginners have problems to understand each single parameter and the effect it has
849 on model results. We compare different models and settings, which helps to decide selecting the
850 best suited approach. and to consider the parameters that have to be adjusted. Afterall, we suggest

31

851 to increase the independent dating density and to adjust prior settings as detailed as possible to
852 gain a more precise chronology for the varve-integration attempt.

853 Optimizing the Holzmaar chronology is the first step in order to provide a precise and robust age-
854 depth model for upcoming and high-resolution multi-proxy investigations to unveil all the
855 environmental details recorded by the varved sediment archive of Holzmaar.

Appendix
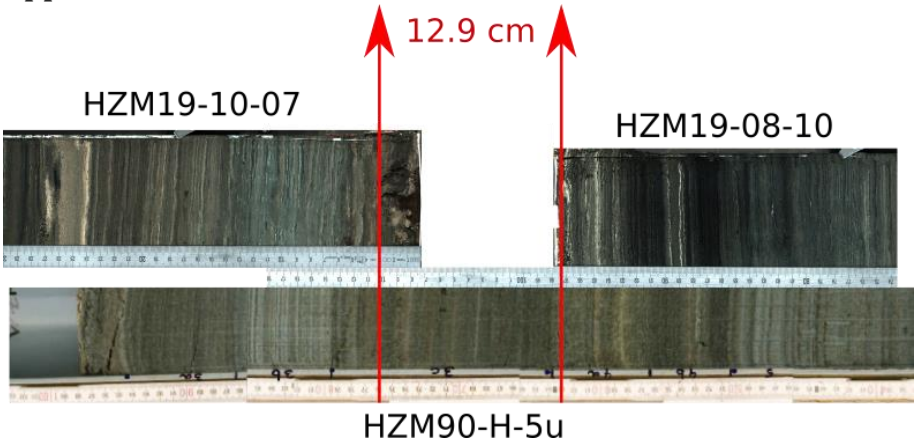
857
858 *Figure A1181: Determination of the technical gap for HZM19 during the YD. This gap exists between sections HZM19-10-*
859 *07 and HZM19-08-10 and is bridged by section HZM90-H5u from an earlier coring campaign.*

860 *coring campaign.*

861

862
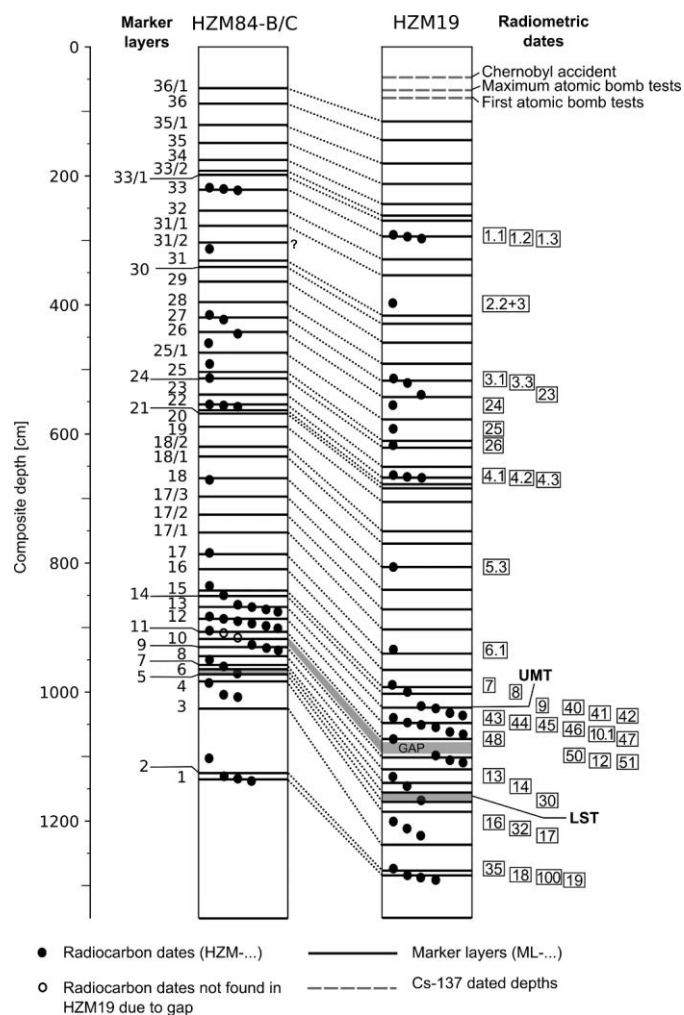
Figure A2: Correlation of HZM84-B/C and HZM19. Positions of marker layers (ML indicated to the left) are marked as solid lines and connected by dotted lines between both profiles. Positions of radiocarbon dates (numbers indicated in rectangular boxes to the right) are marked as solid circles. Grey dotted horizontal lines refer to Cs-137 dated depths. Positions of Ulmener Maar Tephra (UMT), Laacher See Tephra (LST) and the technical gap are indicated.

868
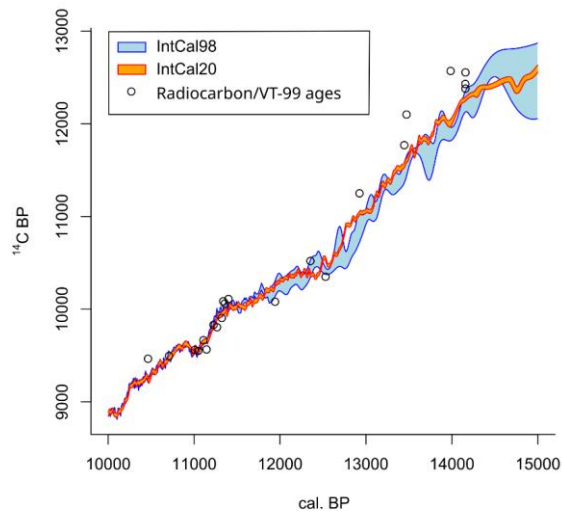
Figure A32: Radiocarbon ages vs. Intcal98 and Intcal20 calibrated ages between 10,000 and 15,000 cal BP. Black circles
show radiocarbon ages from Holzmaar vs. VT-99 age (reworked samples excluded). An underestimation of these ages
occurs after 12,500 cal BP, where VT-99 seems to be too young.

869
870
871

872

873

874
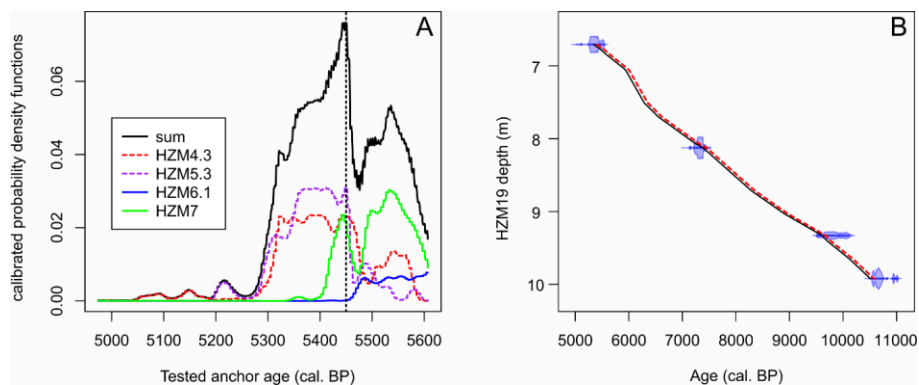
Figure A4: Calculations for the floating VT-99 chronology of Model D, section 3. A: Calculation of the anchoring age for the varve chronology based on matched and summed calibrated probability density function values of all radiocarbon samples within this section. The maximum summed probability occurs at an anchor age of 5450 cal BP. B: Original VT-99 (black line) vs. floating VT-99 (+65 years, red dotted line) with calibrated radiocarbon samples vs. depth.
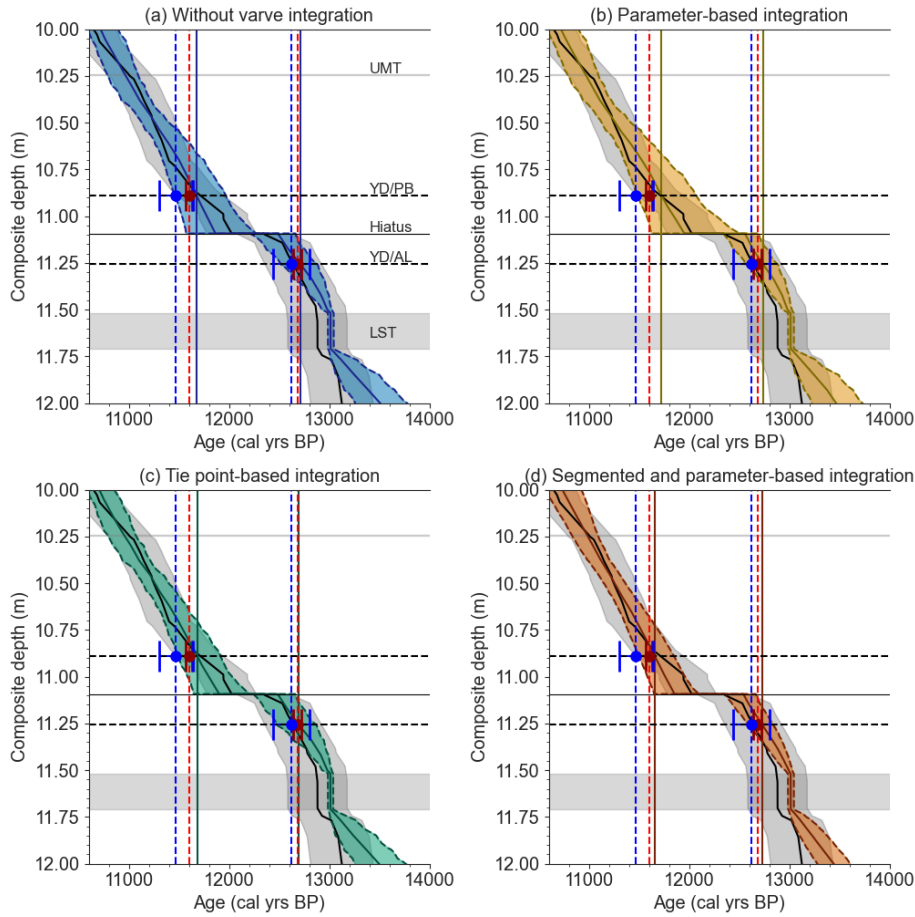
Figure A5: Close-up plots for the Lateglacial / Early Holocene transition for Model A, B, C and D with VT-99 mean age (black solid line) and error (shaded in gray) for comparison. Horizontal lines as labelled in (a). Vertical lines refer to the Younger Dryas transitions for each Model (solid lines), while dotted lines refer to mean ages derived by different sites (Lake Gosciaz in blue: Bonk et al., 2021; Meerfelder Maar in red: Brauer et al., 1999).

Table A1: Core section and composite depths of lithozones H1 to H12 for HZM19

Lithozone	From			To			Biozone	Human phase
	Section	Section depth [mm]	Composite depth [mm]	Section	Section depth [mm]	Composite depth [mm]		
H12	HZM19_07_01	138	11	HZM19_08_01	700	1057	Subatlantic	Last century
H11	HZM19_08_01	700	1058	HZM19_08_03	520	3081	Subatlantic	Middle Ages / Little Ice Age
H10	HZM19_08_03	520	3081	HZM19_08_04	710	4308	Subatlantic	Migration Period / Early Middle Ages
H9	HZM19_08_04	710	4308	HZM19_08_05	750	5535	Subatlantic	Iron Age / Roman Period
H8	HZM19_08_05	750	5535	HZM19_10_05	480	9280	Subboreal/Atlantic	
H7	HZM19_10_05	480	9280	HZM19_11_06	588	9852	Boreal	
H6	HZM19_11_06	588	9852	HZM19_08_10	140	10025	Preboreal	
H5	HZM19_08_10	140	10025	HZM19_08_10	860	10745	Preboreal	
H4	HZM19_08_10	860	10745	HZM19_08_10	970	10855	Preboreal	
H3	HZM19_08_10	970	10855	HZM19_10_07	300	11258	Younger Dryas	
H2	HZM19_10_07	300	11258	HZM19_10_08	859	12859	Bölling/Alleröd	
H1	HZM19_10_08	860	12860	HZM19_07_17	920	14643	Pleniclacial (Late Weichselian)	

890 *Table A221: Error (1 sigma) estimations for different varve quality periods for the Holzmaar record (Zolitschka, 1998b),*
891 *updated from VT-95 to VT-99.*

Varve quality period	VT-99 (duration in years)	Error
A	0 – 2800	±4.0 %
B	2800 – 5300	±2.6 %
C	5300 – 11,600	±0.7 %
D	11,600 – 14,158	±5.9 %
Entire record	0 – 14,158	±2.5 %

892

893

Table A3: List of markers used for correlation of core sections in HZM19

Correlation Marker	Section 1	Section 1 depth (mm)	Section 2	Section 2 depth (mm)
CM_1	HZM19-07-01	970	HZM19-08-01	500
CM_2	HZM19-08-01	755	HZM19-07-02	235
CM_3	HZM19-08-01	795	HZM19-07-02	285
CM_4	HZM19-08-01	935	HZM19-08-02	390
CM_5	HZM19-07-03	230	HZM19-08-02	850
CM_6	HZM19-07-03	585	HZM19-08-03	80
CM_7	HZM19-07-03	665	HZM19-08-03	155
CM_8	HZM19-07-03	925	HZM19-08-03	390
CM_9	HZM19-07-04	30	HZM19-08-03	515
CM_10	HZM19-07-04	45	HZM19-08-03	525
CM_11	HZM19-07-04	85	HZM19-08-03	570
CM_12	HZM19-07-04	155	HZM19-08-03	640
CM_13	HZM19-07-04	255	HZM19-08-03	730
CM_14	HZM19-07-04	800	HZM19-08-04	230
CM_15	HZM19-10-01	90	HZM19-08-04	990
CM_16	HZM19-10-01	290	HZM19-08-05	40
CM_17	HZM19-10-01	320	HZM19-08-05	70
CM_18	HZM19-10-01	340	HZM19-08-05	90
CM_19	HZM19-10-01	410	HZM19-08-05	155
CM_20	HZM19-10-01	670	HZM19-08-05	390
CM_21	HZM19-10-01	925	HZM19-08-05	645
CM_22	HZM19-10-02	60	HZM19-08-05	805
CM_23	HZM19-10-02	180	HZM19-08-05	925
CM_24	HZM19-10-02	245	HZM19-08-05	990
CM_25	HZM19-10-02	570	HZM19-08-06	290
CM_26	HZM19-10-02	815	HZM19-08-06	535
CM_27	HZM19-10-02	990	HZM19-08-06	700
CM_28	HZM19-10-03	10	HZM19-08-06	855
CM_29	HZM19-10-03	790	HZM19-08-07	520
CM_30	HZM19-10-03	830	HZM19-08-07	560
CM_31	HZM19-10-04	180	HZM19-08-07	975
CM_32	HZM19-10-04	320	HZM19-08-08	80
CM_33	HZM19-10-04	425	HZM19-08-08	175
CM_34	HZM19-10-04	505	HZM19-08-08	260
CM_35	HZM19-10-04	870	HZM19-08-08	640
CM_36	HZM19-10-05	150	HZM19-08-08	975
CM_37	HZM19-10-05	850	HZM19-11-06	380
CM_38	HZM19-08-10	135	HZM19-11-06	780
CM_39	HZM19-08-10	180	HZM19-11-06	820
CM_40	HZM19-08-10	355	HZM19-11-06	995
GAP				
CM_41	HZM19-10-07	250	HZM19-11-07	170
CM_42	HZM19-10-07	750	HZM19-11-07	650
CM_43	HZM19-10-07	905	HZM19-11-07	800
CM_44	HZM19-10-07	970	HZM19-11-07	860
CM_45	HZM19-10-08	395	HZM19-11-07	300

Formatiert: Beschriftung, Nicht vom nächsten Absatz trennen

CM_46	HZM19-10-08	580	HZM19-11-08	45
CM_47	HZM19-10-08	620	HZM19-11-08	85
CM_48	HZM19-07-17	100	HZM19-11-08	1250

Table A4 3: Core section depths of the composite profile HZM19 with resulting composite end depths for each core.

Core section	From [mm]	To [mm]	Length [mm]	Composite core section end depth [mm]
HZM19_07_01	138	800	662	662
HZM19_08_01	305	755	451	1113
HZM19_07_02	243	924	681	1794
HZM19_08_02	380	839	459	2254
HZM19_07_03	229	912	683	2936
HZM19_08_03	375	714	339	3275
HZM19_07_04	243	800	557	3833
HZM19_08_04	235	994	759	4592
HZM19_10_01	90	913	823	5415
HZM19_08_05	630	930	299	5715
HZM19_10_02	183	877	693	6409
HZM19_08_06	596	957	361	6770
HZM19_10_03	87	827	740	7510
HZM19_08_07	562	971	409	7919
HZM19_10_04	179	870	691	8611
HZM19_08_08	641	967	326	8937
HZM19_10_05	137	859	722	9659
HZM19_11_06	395	655	260	9919
HZM19_08_10	35	974	939	10859
Technical gap			129	10988
HZM19_10_07	30	810	780	11768
HZM19_11_07	710	1012	302	12071
HZM19_10_08	72	902	830	12902
HZM19_11_08	326	1245	919	13822
HZM19_07_17	100	920	820	14643

Table A52: Marker layers (in italics) and radiocarbon dates (Hajdas et al., 2000, 1995 plus one unpublished radiocarbon date) vs. composite depth of HZM19. The calibrated median ^{14}C age is calculated using OxCal with the IntCal20 calibration curve. Inconsistent calibrated ages are shown in brackets.

Marker layer and ^{14}C sample ID	HZM19 depth (m)	VT-99 Age (cal BP)	VT-99 cumulative ±1σ error (yrs)	^{14}C age (BP)	^{14}C ±1σ error (yrs)	Calibrated ^{14}C median age (cal BP)	^{14}C ±1σ error (yrs)
ML-36/1	*1.16*	*141*	*6*				
ML-36	*1.45*	*209*	*8*				
ML-35/1	*1.81*	*334*	*13*				
ML-35	*2.12*	*442*	*18*				
ML-34	*2.44*	*572*	*23*				
ML-33/2	*2.62*	*657*	*26*				
ML-33/1	*2.69*	*685*	*27*				
HZM-1.1	2.90	796	32	685	40	644	41
HZM-1.2	2.91	802	32	795	40	708	29
HZM-1.3	2.93	810	32	975	90	869	94
ML-33	*2.94*	*819*	*33*				
ML-32	*3.29*	*985*	*39*				
ML-31/1	*3.54*	*1248*	*50*				
HZM-2.2+3	4.01	1569	63	1565	55	1451	57
ML-31	*4.17*	*1710*	*68*				
ML-30	*4.29*	*1789*	*72*				
ML-29	*4.59*	*1984*	*79*				
ML-28	*4.91*	*2219*	*89*				
HZM-3.1	5.16	2433	97	2405	60	2469	112
ML-27	*5.17*	*2449*	*98*				
HZM-3.3*	5.19	2450	98	2750	60	(2850)	66
ML-26	*5.43*	*2593*	*104*				
HZM-23*	5.45	2595	104	2720	60	(2826)	58
HZM-24	5.61	2754	110	2620	65	2743	101
ML-25/1	*5.77*	*3147*	*121*				
HZM-25	5.97	3704	136	3465	70	3730	96
ML-25	*6.11*	*3992*	*143*				
ML-24	*6.21*	*4420*	*154*				
HZM-26*	6.23	4616	159	4100	90	4624	127
ML-23	*6.51*	*5083*	*171*				
ML-22	*6.68*	*5286*	*177*				
HZM-4.1	6.69	5334	177	4575	65	5243	131
HZM-4.2	6.70	5359	177	4730	70	5462	85
HZM-4.3	6.71	5385	178	4675	70	5409	95
ML-21	*6.78*	*5520*	*179*				
ML-20	*6.84*	*5619*	*179*				
ML-19	*7.05*	*5977*	*182*				
ML-18/2	*7.51*	*6328*	*184*				
ML-18/1	*7.70*	*6590*	*186*				
ML-18	*8.06*	*7274*	*191*				
HZM-5.3	8.13	7428	192	6455	70	7363	68
ML-17/3	*8.42*	*7870*	*195*				
ML-17/2	*8.72*	*8338*	*198*				

ML-17/1	*9.03*	*8943*	*203*				
HZM-6.1	9.33	9649	207	8800	95	9851	170
ML-17	*9.40*	*9746*	*208*				
ML-16	*9.66*	*10169*	*211*				
HZM-7	9.92	10464**	213	9465	45	10705	130
ML-15	*9.92*	*10554*	*214*				
ML-14	*10.03*	*10681*	*215*				
HZM-8	10.07	10708	215	9495	55	10773	148
ML-13	*10.24*	*10999*	*217*				
HZM-9 (UMT)	10.25	11008	217	9560	49	10923	121
HZM-40	10.27	11048	217	9550	80	10901	148
HZM-41	10.33	11109	218	9665	100	10998	154
HZM-42	10.38	11145	218	9565	100	10912	160
HZM-43	10.46	11226	219	9830	100	11264	178
ML-12	*10.48*	*11232*	*219*				
HZM-44	10.52	11267	219	9805	190	11243	329
HZM-45	10.59	11322	219	9905	80	11357	138
HZM-46	10.64	11357**	219	10060	80	11584	159
HZM-10.1	10.67	11339**	219	10085	80	11630	165
HZM-47	10.70	11400	220	10110	110	11680	231
ML-11	*10.73*	*11453*	*220*				
HZM-48*	10.78	11534	221	11040	140	(12959)	120
HZM-50	10.99	11942	241	10080	110	11628	214
ML-9	*11.02*	*11943*	*241*				
HZM-12	11.10	12354	266	10520	90	12509	181
HZM-51	11.14	12530	276	10350	90	12203	194
ML-8	*11.20*	*12578*	*279*				
HZM-13*	11.38	12769	290	11295	85	(13197)	74
ML-7	*11.41*	*12778*	*291*				
HZM-14*	11.48	12861	296	11780	100	(13647)	112
ML-6	*11.56*	*12880*	*297*				
ML-5	*11.70*	*12880*	*297*				
HZM-30	11.74	12925	299	11250	110	13158	109
ML-4	*11.86*	*13087*	*309*				
HZM-16*	12.03	13130	311	13140	140	(15766)	212
HZM-32	12.19	13445	330	11770	135	13642	150
HZM-17	12.26	13472	332	12100	110	13984	183
ML-3	*12.40*	*13646***	*339*				
HZM-35	12.78	13985	362	12570	130	14858	286
ML-2	*12.86*	*14152***	*369*				
HZM-18	12.90	14156	372	12430	110	14586	249
ML-1	*12.90*	*14156***	*372*				
HZM-100***	12.92	14157	372	12380	85	14492	228
HZM-19	12.93	14158	372	12555	80	14879	221

* Dates described to contain reworked organic material or being fractionated during graphitization (see Hajdas et al., 1995).

** VT-99 dates excluded from modelling due to inconsistencies in documentation.

*** unpublished radiocarbon age (KIA-1460)

908
909
910
911
912

Table A6: Age estimations for VT-99 and Models A-D with their 95% confidence intervals in brackets for Ulmener Maar Tephra (UMT), Younger Dryas/Preboreal-transition (YD/PB), YD duration, Allerød/Younger Dryas-transition (AL/YD), predicted YD hiatus with duration and position, Laacher See Tephra (LST), Maximum model age at 12.93 m with its mean and maximum age ranges and position of the maximum age range and maximum difference between VT-99 and each of the model ranges.

Chronology	VT-99	A	B	C	D
Age of UMT	10999 [10782, 11216]	10961 [10784, 11090]	10965 [10787, 11093]	10952 [10788, 11067]	10981 [10829, 11088]
YD/PB transition	11632	11674 [11461, 11965]	11723 [11486, 12070]	11682 [11494, 11913]	11655 [11499, 11845]
YD duration	974	1038	1014	1012	1073
AL/YD transition	12606	12712 [12517, 12880]	12737 [12562, 12880]	12694 [12475, 12869]	12728 [12595, 12838]
Duration of YD hiatus	320	623	603	583	686
End of YD hiatus	12025	11863 [11571, 12269]	11952 [11623, 12502]	11901 [11646, 12207]	11854 [11651, 12098]
Age of LST	12880 [12583, 13177]	13010 [12984, 13042]	13010 [12985, 13043]	13009 [12984, 13037]	13011 [12984, 13043]
Maximum model age (at 12.93 m)	14158 [13786, 14530]	14615 [14339, 14926]	14456 [14236, 14749]	14614 [14332, 14919]	14485 [14287, 14721]
Mean age range	282	468	456	329	229
Maximum age range	744	1056	1064	749	447
Max. age range position (m)	12.93	8.86	8.78	9.18	11.09
Maximum difference to VT-99 age range	0	655	665	401	0

913

914

915 *Table A75: Additional dates for the HZM19 chronology with composite depths, ages (cal. BP) and errors used for Bacon*
916 *calculations. LST age with error is from Reinig et al. (2020).*

Event	HZM19 comp. depth (cm)	Age (cal. BP)	error
Sediment surface	0.00	-69	1
Chernobyl accident	47.20*	-36	1
Maximum atomic bomb tests	67.20*	-13	1
First atomic bomb tests	79.20*	0	1
Laacher See Tephra	1160.00	13,006	9

917 ** 22 cm subtracted due to slump event documented by Pb-210 data.*

918

Data Availability

The results of the different age-depth models carried out for the lacustrine sediment record

from Holzmaar are accessible via the PANGAEA data archiving and publication system at

https://doi.org/10.1594/PANGAEA.949393~~https://doi.org/10.1594/PANGAEA.xxxxxx~~.

Author contributions

SB and BZ conducted the fieldwork and conceptualized the study. SB described and sampled the
sediment, modified and run the Bayesian age-depth models, visualized the data and drafted the
first version of the manuscript. WT measured and interpreted lead and cesium data. All authors
contributed to the writing and to revising of the manuscript.

Competing interests

The contact author declares that neither she nor her co-authors have any competing interests.

Disclaimer

Acknowledgments

We like to thank Christian Ohlendorf, Rafael Stiens and An-Sheng Lee for participating in the
coring campaign of 2019 and also for subsequent help with core opening, sediment preparations
and scanning in the GEOPOLAR lab. Furthermore, we want to thank Maarten Blaauw, Arne
Ramisch and Alicja Bonk for helpful discussions.

References

Anderson, R. Y. and Dean, W. E.: Lacustrine varve formation through time, Palaeogeogr. Palaeocl., 62, 215–235, https://doi.org/10.1016/0031-0182(88)90055-7, 1988.

Baier, J., Lücke, A., Negendank, J. F. W., Schleser, G.-H., and Zolitschka, B.: Diatom and geochemical evidence of mid- to late Holocene climatic changes at Lake Holzmaar, West-Eifel (Germany), Quatern. Int., 113, 81–96, https://doi.org/10.1016/S1040-6182(03)00081-8, 2004.

Battarbee, R. W., Howells, G. D., Skeffington, R. A., Bradshaw, A. D., Battarbee, R. W., Mason, B. J., Renberg, I., and Talling, J. F.: The causes of lake acidification, with special reference to the role of acid deposition, Philos. T. Roy. Soc. B., 327, 339–347, https://doi.org/10.1098/rstb.1990.0071, 1990.

Berglund, B. E. (Ed.): Handbook of Holocene Palaeoecology and Palaeohydrology, John Wiley & Sons Ltd., Chichester, 869 pp., 1986.

Blaauw, M.: Methods and code for 'classical' age-modelling of radiocarbon sequences, Quat. Geochronol., 5, 512–518, https://doi.org/10.1016/j.quageo.2010.01.002, 2010.

950 Blaauw, M. and Christen, J. A.: Flexible paleoclimate age-depth models using an autoregressive
951 gamma process, Bayesian Anal., 6, 457–474, https://doi.org/10.1214/11-BA618, 2011.

952 Blaauw, M., Christen, J. A., Bennett, K. D., and Reimer, P. J.: Double the dates and go for Bayes —
953 Impacts of model choice, dating density and quality on chronologies, Quaternary Sci. Rev., 188,
954 58–66, https://doi.org/10.1016/j.quascirev.2018.03.032, 2018.

955 Blaauw, M., Christen, J. A., Lopez, M. A. A., Vazquez, J. E., V, O. M. G., Belding, T., Theiler, J., Gough,
956 B., and Karney, C.: rbacon: Age-Depth Modelling using Bayesian Statistics, CRAN [code], 2021.

957 Bonk, A., Müller, D., Ramisch, A., Kramkowski, M. A., Noryśkiewicz, A. M., Sekudewicz, I.,
958 Gąsiorowski, M., Luberda-Durnaś, K., Słowiński, M., Schwab, M., Tjallingii, R., Brauer, A., and
959 Błaszkiewicz, M.: Varve microfacies and chronology from a new sediment record of Lake Gościąż
960 (Poland), Quaternary Sci. Rev., 251, 106715, https://doi.org/10.1016/j.quascirev.2020.106715,
961 2021.

962 Brauer, A.: Weichselzeitliche Seesedimente des Holzmaars - Warvenchronologie des Hochglazials
963 und Nachweis von Klimaschwankungen, Ph.D. thesis, Universität Trier, Documenta naturae, 85,
964 1–210, 1994.

965 Brauer, A., Hajdas, I., Negendank, J. F. W., Rein, B., Vos, H., and Zolitschka, B.: Warvenchronologie -
966 eine Methode zur absoluten Datierung und Rekonstruktion kurzer und mittlerer solarer
967 Periodizitäten, Geowissenschaften, 12, 325–332, 1994.

968 Brauer, A., Endres, C., Günter, C., Litt, T., Stebich, M., and Negendank, J. F. W.: High resolution
969 sediment and vegetation responses to Younger Dryas climate change in varved lake sediments
970 from Meerfelder Maar, Germany, Quaternary Sci. Rev., 18, 321–329,
971 https://doi.org/10.1016/S0277-3791(98)00084-5, 1999.

972 Bronk Ramsey, C.: Deposition models for chronological records, Quaternary Sci. Rev., 27, 42–60,
973 https://doi.org/10.1016/j.quascirev.2007.01.019, 2008.

974 Brooks, S. P. and Gelman, A.: General Methods for Monitoring Convergence of Iterative
975 Simulations, J. Comput. Graph. Stat., 7, 434–455,
976 https://doi.org/10.1080/10618600.1998.10474787, 1998.

977 Büchel, G.: Maars of the Westeifel, Germany, in: Paleolimnology of European Maar Lakes, edited
978 by: Negendank, J. F. W. and Zolitschka, B., Springer, Berlin, Heidelberg, 1–13,
979 https://doi.org/10.1007/BFb0117585, 1993.

980 Cohen, A. S.: Paleolimnology. The history and evolution of lake systems, Oxford University Press,
981 Oxford, 500 pp., 2003.

982 Davies, S. M.: Cryptotephras: the revolution in correlation and precision dating, Journal of
983 Quaternary Science, 30, 114–130, https://doi.org/10.1002/jqs.2766, 2015.

984 De Geer, G.: A geochronology of the last 12,000 years., Eleventh International Geological Congress,
985 Stockholm, 1, 241–253, 1912.

986 Dean, W. E., Bradbury, J. P., Anderson, R. Y., and Barnosky, C. W.: The Variability of Holocene
987 Climate Change: Evidence from Varved Lake Sediments, Science, 226, 1191–1194,
988 https://doi.org/10.1126/science.226.4679.1191, 1984.

989 Fortin, D., Praet, N., McKay, N. P., Kaufman, D. S., Jensen, B. J. L., Haeussler, P. J., Buchanan, C., and
990 De Batist, M.: New approach to assessing age uncertainties – The 2300-year varve chronology

991   from Eklutna Lake, Alaska (USA), Quaternary Sci. Rev., 203, 90–101,
992   https://doi.org/10.1016/j.quascirev.2018.10.018, 2019.

993   García, M. L., Birlo, S., and Zolitschka, B.: Paleoenvironmental changes of the last 16,000 years
994   based on diatom and geochemical stratigraphies from the varved sediment of Holzmaar (West-
995   Eifel Volcanic Field, Germany), Quaternary Science Reviews, 293, 107691,
996   https://doi.org/10.1016/j.quascirev.2022.107691, 2022.

997   Goslar, T., Kuc, T., Ralska-Jasiewiczowa, M., Rózánski, K., Arnold, M., Bard, E., van Geel, B., Pazdur,
998   M., Szeroczyńska, K., Wicik, B., Więckowski, K., and Walanus, A.: High-resolution lacustrine record
999   of the late glacial/holocene transition in central Europe, Quaternary Sci. Rev., 12, 287–294,
1000   https://doi.org/10.1016/0277-3791(93)90037-M, 1993.

1001   Hajdas, I., Zolitschka, B., Ivy-Ochs, S. D., Beer, J., Bonani, G., Leroy, S. A. G., Negendank, J. W.,
1002   Ramrath, M., and Suter, M.: AMS radiocarbon dating of annually laminated sediments from lake
1003   Holzmaar, Germany, Quaternary Sci. Rev., 14, 137–143, https://doi.org/10.1016/0277-
1004   3791(94)00123-S, 1995.

1005   Hajdas, I., Bonani, G., and Zolitschka, B.: Radiocarbon Dating of Varve Chronologies: Soppensee
1006   and Holzmaar Lakes after Ten Years, Radiocarbon, 42, 349–353,
1007   https://doi.org/10.1017/S0033822200030290, 2000.

1008   Hajdas-Skowronek, I.: Extension of the radiocarbon calibration curve by AMS dating of laminated
1009   sediments of Lake Soppensee and Lake Holzmaar, Ph. D thesis, ETH Zurich,
1010   https://doi.org/10.3929/ETHZ-A-000916163, 1993.

1011   Haslett, J. and Parnell, A.: A simple monotone process with application to radiocarbon-dated depth
1012   chronologies, J. R. Stat. Soc. C.-Appl., 57, 399–418, https://doi.org/10.1111/j.1467-
1013   9876.2008.00623.x, 2008.

1014   Jenny, J.-P., Koirala, S., Gregory-Eaves, I., Francus, P., Niemann, C., Ahrens, B., Brovkin, V., Baud, A.,
1015   Ojala, A. E. K., Normandeau, A., Zolitschka, B., and Carvalhais, N.: Human and climate global-scale
1016   imprint on sediment transfer during the Holocene, P. Natl. Acad. Sci., 116, 22972–22976,
1017   https://doi.org/10.1073/pnas.1908179116, 2019.

1018   Kelts, K., Briegel, U., Ghilardi, K., and Hsu, K.: The limnogeology-ETH coring system, Schweiz. Z.
1019   Hydro., 48, 104–115, https://doi.org/10.1007/BF02544119, 1986.

1020   Kienel, U., Schwab, M. J., and Schettler, G.: Distinguishing climatic from direct anthropogenic
1021   influences during the past 400 years in varved sediments from Lake Holzmaar (Eifel, Germany), J.
1022   Paleolimnol., 33, 327–347, https://doi.org/10.1007/s10933-004-6311-z, 2005.

1023   Lacourse, T. and Gajewski, K.: Current practices in building and reporting age-depth models,
1024   Quaternary Res., 96, 28–38, https://doi.org/10.1017/qua.2020.47, 2020.

1025   Lamoureux, S.: Varve Chronology Techniques, in: Tracking Environmental Change Using Lake
1026   Sediments: Basin Analysis, Coring, and Chronological Techniques, edited by: Last, W. M. and Smol,
1027   J. P., Springer Netherlands, Dordrecht, 247–260, https://doi.org/10.1007/0-306-47669-X_11,
1028   2001.

1029   Last, W. M. and Smol, J. P. (Eds.): Tracking Environmental Change Using Lake Sediments, vol. 1,
1030   Basin Analysis, Coring, and Chronological Techniques, Springer Netherlands, Dordrecht, 548 pp.,
1031   2001a.

Last, W. M. and Smol, J. P. (Eds.): Tracking Environmental Change Using Lake Sediments, vol. 2, Physical and Geochemical Methods, Springer Netherlands, Dordrecht, 504 pp., 2001b.

Leroy, S. A. G., Zolitschka, B., Negendank, J. F. W., and Seret, G.: Palynological analyses in the laminated sediment of Lake Holzmaar (Eifel, Germany): duration of Lateglacial and Preboreal biozones, Boreas, 29, 52–71, https://doi.org/10.1111/j.1502-3885.2000.tb01200.x, 2000.

Litt, T., Schölzel, C., Kühl, N., and Brauer, A.: Vegetation and climate history in the Westeifel Volcanic Field (Germany) during the past 11 000 years based on annually laminated lacustrine maar sediments, Boreas, 38, 679–690, https://doi.org/10.1111/j.1502-3885.2009.00096.x, 2009.

Lorenz, V.: Explosive Volcanism of the West Eifel Volcanic Field/Germany, in: Developments in Petrology, vol. 11, edited by: Kornprobst, J., Elsevier, 299–307, https://doi.org/10.1016/B978-0-444-42273-6.50026-2, 1984.

Lorenz, V., Lange, T., and Büchel, G.: Die Vulkane der Westeifel, Jahresberichte und Mitteilungen des Oberrheinischen Geologischen Vereins, 102, 379–411, https://doi.org/10.1127/jmogv/102/0022, 2020.

Lotter, A. F.: Absolute Dating of the Late-Glacial Period in Switzerland Using Annually Laminated Sediments, Quaternary Res., 35, 321–330, https://doi.org/10.1016/0033-5894(91)90048-A, 1991.

Lücke, A., Schleser, G. H., Zolitschka, B., and Negendank, J. F. W.: A Lateglacial and Holocene organic carbon isotope record of lacustrine palaeoproductivity and climatic change derived from varved lake sediments of Lake Holzmaar, Germany, Quaternary Sci. Rev., 22, 569–580, https://doi.org/10.1016/S0277-3791(02)00187-7, 2003.

Martin-Puertas, C., Walsh, A. A., Blockley, S. P. E., Harding, P., Biddulph, G. E., Palmer, A., Ramisch, A., and Brauer, A.: The first Holocene varve chronology for the UK: Based on the integration of varve counting, radiocarbon dating and tephrostratigraphy from Diss Mere (UK), Quat. Geochronol., 61, 101134, https://doi.org/10.1016/j.quageo.2020.101134, 2021.

Meyer, W.: Zur Entstehung der Maare in der Eifel, Z. Dtsch. Ges. Geowiss., 141–155, https://doi.org/10.1127/zdgg/136/1985/141, 1985.

Meyer, W.: Geologie der Eifel, 4th ed., Schweizerbart Science Publishers, Stuttgart, Germany, 2013.

Meyer, W. and Stets, J.: Pleistocene to Recent tectonics in the Rhenish Massif (Germany), Neth. J. Geosci., 81, 217–221, https://doi.org/10.1017/S0016774600022460, 2002.

Muggeo, V. M. R.: segmented: Regression Models with Break-Points / Change-Points Estimation, CRAN [code], 2022.

Nesje, A., Søgnen, K., Elgersma, A., and Dahl, S. O.: A Piston Corer for Lake Sediments, Norsk. Geogr. Tidsskr., 41, 123–125, https://doi.org/10.1080/00291958708621986, 1987.

Olsson, I. U.: Radiometric dating, John Wiley and Sons, United Kingdom, 1986.

O'Sullivan, P. E.: Annually-laminated lake sediments and the study of Quaternary environmental changes — a review, Quaternary Sci. Rev., 1, 245–313, https://doi.org/10.1016/0277-3791(83)90008-2, 1983.

Pearson, G. W., Pilcher, J. R., Baillie, M. G. L., and Hillam, J.: Absolute radiocarbon dating using a low altitude European tree-ring calibration, Nature, 270, 25–28, https://doi.org/10.1038/270025a0, 1977.

Prasad, S. and Baier, J.: Tracking the impact of mid- to late Holocene climate change and anthropogenic activities on Lake Holzmaar using an updated Holocene chronology, Global Planet. Change, 122, 251–264, https://doi.org/10.1016/j.gloplacha.2014.08.020, 2014.

R Core Team: R: A Language and Environment for Statistical Computing, 2021.

Reimer, P. J., Austin, W. E. N., Bard, E., Bayliss, A., Blackwell, P. G., Bronk Ramsey, C., Butzin, M., Cheng, H., Edwards, R. L., Friedrich, M., Grootes, P. M., Guilderson, T. P., Hajdas, I., Heaton, T. J., Hogg, A. G., Hughen, K. A., Kromer, B., Manning, S. W., Muscheler, R., Palmer, J. G., Pearson, C., van der Plicht, J., Reimer, R. W., Richards, D. A., Scott, E. M., Southon, J. R., Turney, C. S. M., Wacker, L., Adolphi, F., Büntgen, U., Capano, M., Fahrni, S. M., Fogtmann-Schulz, A., Friedrich, R., Köhler, P., Kudsk, S., Miyake, F., Olsen, J., Reinig, F., Sakamoto, M., Sookdeo, A., and Talamo, S.: The INTCAL20 Northern Hemisphere Radiocarbon Age Calibration Curve (0–55 cal kBP), Radiocarbon, 62, 725–757, https://doi.org/10.1017/RDC.2020.41, 2020.

Reinig, F., Wacker, L., Jöris, O., Oppenheimer, C., Guidobaldi, G., Nievergelt, D., Adolphi, F., Cherubini, P., Engels, S., Esper, J., Land, A., Lane, C., Pfanz, H., Remmele, S., Sigl, M., Sookdeo, A., and Büntgen, U.: Precise date for the Laacher See eruption synchronizes the Younger Dryas, Nature, 595, 66–69, https://doi.org/10.1038/s41586-021-03608-x, 2021.

Renberg, I. and Hansson, H.: A pump freeze corer for recent sediments, Limnol. Oceanogr., 38, 1317–1321, https://doi.org/10.4319/lo.1993.38.6.1317, 1993.

Renberg, I., Persson, M. W., and Emteryd, O.: Pre-industrial atmospheric lead contamination detected in Swedish lake sediments, Nature, 368, 323–326, https://doi.org/10.1038/368323a0, 1994.

Saarnisto, M.: Long varve series in Finland, Boreas, 14, 133–137, https://doi.org/10.1111/j.1502-3885.1985.tb00905.x, 1985.

Saarnisto, M.: Annually laminated lake sediments, in: Handbook of Holocene palaeoecology and palaeohydrology, edited by: Berglund, B. E., John Wiley and Sons Ltd, Chichester, 343–370, 1986.

Scharf, B.: Limnologische Beschreibung, Nutzung und Unterhaltung von Eifelmaaren, Ministerium für Umwelt und Gesundheit Rheinland-Pfalz, Mainz, 1987.

Scharf, B. W. and Oehms, M.: Physical and chemical characteristics, in: Limnology of Eifel maar lakes. Ergebnisse der Limnologie, vol. 38, edited by: Scharf, B. W. and Björk, S., E. Schweizerbart, Stuttgart, 63–83, 1992.

Schmincke, H.-U.: The Quaternary Volcanic Fields of the East and West Eifel (Germany), in: Mantle Plumes: A Multidisciplinary Approach, edited by: Ritter, J. R. R. and Christensen, U. R., Springer, Berlin, Heidelberg, 241–322, https://doi.org/10.1007/978-3-540-68046-8_8, 2007.

Schmincke, H.-U.: Vulkane der Eifel, 2nd ed., Springer, Berlin, Heidelberg, 2014.

Schnurrenberger, D., Russell, J., and Kelts, K.: Classification of lacustrine sediments based on sedimentary components, J. Paleolimnol., 29, 141–154, https://doi.org/10.1023/A:1023270324800, 2003.

Shanahan, T. M., Beck, J. W., Overpeck, J. T., McKay, N. P., Pigati, J. S., Peck, J. A., Scholz, C. A., Heil, C. W., and King, J.: Late Quaternary sedimentological and climate changes at Lake Bosumtwi Ghana: New constraints from laminae analysis and radiocarbon age modeling, Palaeogeogr. Palaeocl., 361–362, 49–60, https://doi.org/10.1016/j.palaeo.2012.08.001, 2012.

1114 Sirocko, F., Dietrich, S., Veres, D., Grootes, P. M., Schaber-Mohr, K., Seelos, K., Nadeau, M.-J., Kromer,
1115 B., Rothacker, L., Röhner, M., Krbetschek, M., Appleby, P., Hambach, U., Rolf, C., Sudo, M., and Grim,
1116 S.: Multi-proxy dating of Holocene maar lakes and Pleistocene dry maar sediments in the Eifel,
1117 Germany, Quaternary Sci. Rev., 62, 56–76, https://doi.org/10.1016/j.quascirev.2012.09.011,
1118 2013.

1119 Stuiver, M., Reimer, P. J., Bard, E., Beck, J. W., Burr, G. S., Hughen, K. A., Kromer, B., McCormac, G.,
1120 Van Der Plicht, J., and Spurk, M.: INTCAL98 Radiocarbon Age Calibration, 24,000–0 cal BP,
1121 Radiocarbon, 40, 1041–1083, https://doi.org/10.1017/S0033822200019123, 1998.

1122 Telford, R., Heegaard, E., and Birks, H.: All age–depth models are wrong: but how badly?,
1123 Quaternary Sci. Rev., 23, 1–5, https://doi.org/10.1016/j.quascirev.2003.11.003, 2004.

1124 Trachsel, M. and Telford, R. J.: All age–depth models are wrong, but are getting better, Holocene,
1125 27, 860–869, https://doi.org/10.1177/0959683616675939, 2017.

1126 Turkey, C. S. M. and Lowe, J. J.: Tephrochronology, in: Tracking Environmental Change Using Lake
1127 Sediments: Basin Analysis, Coring, and Chronological Techniques, edited by: Last, W. M. and Smol,
1128 J. P., Springer Netherlands, Dordrecht, 451–471, https://doi.org/10.1007/0-306-47669-X_16,
1129 2001.

1130 Vandergoes, M. J., Howarth, J. D., Dunbar, G. B., Turnbull, J. C., Roop, H. A., Levy, R. H., Li, X., Prior,
1131 C., Norris, M., Keller, L. D., Baisden, W. T., Ditchburn, R., Fitzsimons, S. J., and Bronk Ramsey, C.:
1132 Integrating chronological uncertainties for annually laminated lake sediments using layer
1133 counting, independent chronologies and Bayesian age modelling (Lake Ohau, South Island, New
1134 Zealand), Quaternary Sci. Rev., 188, 104–120, https://doi.org/10.1016/j.quascirev.2018.03.015,
1135 2018.

1136 Wright, H. E., Mann, D. H., and Glaser, P. H.: Piston Corers for Peat and Lake Sediments, Ecology,
1137 65, 657–659, https://doi.org/10.2307/1941430, 1984.

1138 Zolitschka, B.: Spätquartäre Sedimentationsgeschichte des Meerfelder Maares (Westeifel).
1139 Mikrostratigraphie jahreszeitlich geschichteter Seesedimente, E&G Quaternary Sci. J., 38, 87–93,
1140 https://doi.org/10.3285/eg.38.1.08, 1988.

1141 Zolitschka, B.: Jahreszeitlich geschichtete Seesedimente aus dem Holzmaar und dem Meerfelder
1142 Maar, Z. Dtsch. Ges. Geowiss., 25–33, https://doi.org/10.1127/zdgg/140/1989/25, 1989.

1143 Zolitschka, B.: Jahreszeitlich geschichtete Seesedimente ausgewählter Eifelmaare -
1144 paläolimnologische Untersuchung als Beitrag zur spät- und postglazialen Klima- und
1145 Besiedlungsgeschichte, Ph.D. thesis, Universität Trier, Documenta naturae, 60, 226, 1990.

1146 Zolitschka, B.: Absolute dating of late Quaternary Lacustrine sediments by high resolution varve
1147 chronology, 214, 59–61, https://doi.org/10.1007/BF00050932, 1991.

1148 Zolitschka, B.: Climatic change evidence and lacustrine varves from maar lakes, Germany, Clim.
1149 Dynam., 6, 229–232, https://doi.org/10.1007/BF00193535, 1992.

1150 Zolitschka, B.: A 14,000 year sediment yield record from western Germany based on annually
1151 laminated lake sediments, Geomorphology, 22, 1–17, https://doi.org/10.1016/S0169-
1152 555X(97)00051-2, 1998a.

1153 Zolitschka, B.: Paläoklimatische Bedeutung laminierter Sedimente: Holzmaar (Eifel, Deutschland),
1154 Lake C2 (Northwest-Territorien, Kanada) und Lago Grande di Monticchio (Basilicata, Italien),
1155 Habil. thesis, Universität Potsdam, Relief Boden Paläoklima, 13, 176, 1998b.

1156   Zolitschka, B., Haverkamp, B., and Negendank, J. F. W.: Younger Dryas Oscillation — Varve Dated
1157   Microstratigraphic, Palynological and Palaeomagnetic Records from Lake Holzmaar, Germany, in:
1158   The Last Deglaciation: Absolute and Radiocarbon Chronologies, edited by: Bard, E. and Broecker,
1159   W. S., Springer Berlin Heidelberg, Berlin, Heidelberg, 81–101, https://doi.org/10.1007/978-3-
1160   642-76059-4_6, 1992.

1161   Zolitschka, B., Brauer, A., Negendank, J. F. W., Stockhausen, H., and Lang, A.: Annually dated late
1162   Weichselian continental paleoclimate record from the Eifel, Germany, Geology, 28, 783–786,
1163   https://doi.org/10.1130/0091-7613(2000)28<783:ADLWCP>2.0.CO;2, 2000.

1164   Zolitschka, B., Francus, P., Ojala, A. E. K., and Schimmelmann, A.: Varves in lake sediments – a
1165   review, Quaternary Sci. Rev., 117, 1–41, https://doi.org/10.1016/j.quascirev.2015.03.019, 2015.

1166